Choice of Parameters for the Lower Hybrid Heating Experiment for ASDEX

F. Leuterer

IPP 4/202 Juni 1981

MAX-PLANCK-INSTITUT FÜR PLASMAPHYSIK

8046 GARCHING BEI MÜNCHEN

MAX-PLANCK-INSTITUT FÜR PLASMAPHYSIK

GARCHING BEI MÜNCHEN

Choice of Parameters for the Lower Hybrid Heating Experiment for ASDEX

F. Leuterer

IPP 4/202 Juni 1981

Die nachstehende Arbeit wurde im Rahmen des Vertrages zwischen dem Max-Planck-Institut für Plasmaphysik und der Europäischen Atomgemeinschaft über die Zusammenarbeit auf dem Gebiete der Plasmaphysik durchgeführt.

IPP 4/202 F. Leuterer

Choice of Parameters for the Lower Hybrid Heating Experiment for ASDEX

Juni 1981 (in English)

Abstract

The design criteria are described which lead to the choice of frequency and wave-number spectra for the lower hybrid heating experiment be applied on ASDEX.

Choice of Parameters for the Lower Hybrid Heating Experiment for ASDEX.

1.) The physics of lower hybrid heating

a) Plane plasma

The lower hybrid frequency,

$$\omega_{LH} \approx \left[\sum_i \omega_{pi}^2 / (1 + \omega_{pe}^2 / \omega_{ce}^2) \right]^{1/2} \qquad (1)$$

(ω_{pi} = ion plasma frequency, ω_{pe} = electron plasma frequency, ω_{ce} = electron cyclotron frequency; the sum is taken over all ion species),

is a resonance frequency of a cold anisotropic plasma, where the component $\varepsilon_\perp$ of the dielectric tensor $\overline{\overline{\varepsilon}}$ vanishes. For a given frequency $\omega = \omega_{LH}$ and given magnetic field, eq. (1) also defines the electron density n_{LH} at which the lower hybrid resonance occurs. The indices $\perp$ and $\parallel$ refer to the direction of the magnetic field. Near this frequency the phase velocity and group-velocity of the extraordinary electromagnetic wave are very small and comparable to the ion thermal velocity. Therefore, effective interaction between wave and particles can be expected. The theory of wave propagation and heating in this frequency range is treated by numerous authors. A survey can be found in the papers by M. Brambilla /1/ and A. Bers /2/.

The component $N_{\parallel}$ of the wave refractive index ($\vec{N} = \vec{k}\, c/\omega$) determines the propagation of the wave from the antenna into a plasma with increasing density. This is sketched in fig. 1 where $N_{\perp}^2$ is shown as a function of the density with $N_{\parallel}$ as a parameter /1/. The two curves $N_{\perp 1}^2$ and $N_{\perp 2}^2$ are the solutions of the electromagnetic dispersion relation in a cold plasma (ordinary and extraordinary modes). In fig. 1a we have $0 < N_{\parallel} < 1$. Only for very low density we find $N_{\perp}^2$ positive. Therefore the waves cannot penetrate into the dense plasma and remains at the surface. In fig. 1b we have $1 < N_{\parallel} < N_{\parallel crit}$. In this case the waves, after tunneling through a very narrow cutoff layer at the plasma edge, can penetrate into the plasma until they reach a density layer n_A where both electromagnetic modes $N_{\perp 1}^2$ and $N_{\perp 2}^2$ are coupled. The density n_A at this point can be calculated from

$$A = \frac{1}{BC}\left[\frac{N_{\parallel}}{\sqrt{BC}} - \sqrt{N_{\parallel}^2\left(\frac{1}{BC} - 1\right) + 1}\right]^2 \qquad (2)$$

where $A = \omega_{pe}^2/\omega_{ce}^2$; $B = \sum_i \omega_{pi}^2/\omega_{pe}^2 = \sum_i \frac{z_i^2 n_i m_e}{n_e m_i}$

and $C = \omega_{ce}^2/\omega^2$.

For higher densities $N_{\perp 1}^2$ and $N_{\perp 2}^2$ become conjugate complex, i.e. a wave penetrating into the plasma along the dispersion curve $N_{\perp 1}^2$ until it reaches the layer n_A, turns back towards the plasma edge along the dispersion curve $N_{\perp 2}^2$.

Only if $N_{\parallel} < N_{\parallel crit}$, as in fig. 1c, this coupling disappears and the wave $N_{\perp 1}^2$ can reach the lower hybrid resonance at n_{LH}. The value of $N_{\parallel crit}$ has been given by V. Golant /3/:

$$N_{\parallel crit}^2 = \frac{1}{1 - \omega^2/\omega_{ce}\omega_{ci}} = 1 + \omega_{pe}^2/\omega_{ce}^2 \Big|_{Res.} \qquad (3)$$

We recognize from this formula that lower hybrid heating is possible only by means of retarded waves with $N_{\parallel} > 1$.

In a hot plasma the resonance at the lower hybrid frequency disappears and instead the wave experiences a mode conversion into an electrostatic Ion-Bernstein-Wave (dispersion curve 3 in fig. 1c), which is absorbed in the region between the nearest ion cyclotron harmonics. In a tokamak plasma these are in the immediate vicinity of the mode conversion point and therefore we can for the purpose of designing an l.h. experiment consider this region as the volume where the wave energy is absorbed. From the electrostatic dispersion relation, valid in this region, we can derive the density at the mode conversion point, from which - for given density- and temperature profiles - the energy deposition profile can be determined /4/. The density at the mode conversion point is given by

$$\omega_{pe}^2 = \left[\left(\frac{1}{\omega^2}\sum_i \omega_{pi}^2/\omega_{pe}^2 - 1/\omega_{ce}^2\right) + N_{\parallel}\sqrt{\frac{3\beta e^2}{\omega_{ce}^2} + \frac{12}{\omega^4}\sum_i \frac{\omega_{pi}^2}{\omega_{pe}^2}\beta_i^2}\right]^{-1} \qquad (4)$$

with $\beta_j^2 = \kappa T_j/m_j c^2$.

The first term in brackets represents the cold plasma lower hybrid resonance, while the second term, which is proportional to $N_{\parallel}\sqrt{T}$, describes the reduction of the mode conversion density n_{Mc} with respect to the cold plasma resonant density n_{LH}. The requirements for $N_{\parallel}$ are thus less critical then expressed by eq. (3). For the basic design of an experiment we consider it sufficient to require that the accessible density according to eq. (2) coincides with the mode conversion density, eq. (4). More detailed electromagnetic calculations, including first order temperature terms, show only minor differences.

The detailed absorption mechanism, i.e. the question whether mode conversion with cyclotron harmonic damping or stochastic ion heating prevails, is still in discussion. However, in both these schemes the absorption occurs mainly in the mode conversion region and therefore the use of eq. (4) is justified for the design of an experiment. Only for the case that electrons should be heated through electron Landau damping we have to use other design criteria as described in chapter 4.

b) Toroidal plasma

Equations (2) to (4) have been derived from the dispersion relations for plane waves in a homogeneous plasma with a homogeneous magnetic field. Applied locally to an inhomogeneous plasma, we get a first order design for an experiment.

However, the toroidal geometry of a tokamak and the shear in the magnetic field due to the Ohmic heating current influence the wave propagation /5, 6/. In this situation the wave vector components k_Θ and k_Φ (with respect to the tokamak geometry), which are excited by a coupler at the boundary of the plasma, are no longer identical to the wave vector components $k_\parallel$ and $k_\perp$ (with respect to the local magnetic field). Due to the varying magnetic field, $k_\parallel$ and $k_\perp$ do not remain constant as the wave penetrates into a tokamak plasma. Therefore the coupler spectrum, as obtained from plane geometry considerations, has to be reexamined. There is no analytic solution to this problem. However, numerical ray tracing calculations yield satisfactory information /13/.

2.) Plasma- and machine parameters used for the design

For the design of the lower hybrid heating system for ASDEX, we start from the following machine data:

toroidal magnetic field B_o = 25 kG

(max. 28 kG for 5 sec)

Major radius R = 165 cm

minor radius a = 40 cm (for circular cross-section)

Plasma current I_p = 300 kA (max. 500 kA)

gases: hydrogen, deuterium or a mixture thereof

Ohmic heating power $\lesssim$ 600 kW

Plasma lifetime: several seconds.

For the plasma data we assume:

electron density: $3 \cdot 10^{13} \lesssim n_e(0) \lesssim 2 \cdot 10^{14}$ cm^{-3}

temperatures $T_e(0) \approx T_i(0) \approx$ 500 eV

(with 2 MW neutral injection: $T_i(0) \approx$ 1.3 - 2 keV)

impurities: $Z_{eff} < 1.5$

density gradient outside of the magnetic limiter:

$$\nabla n_e \approx \text{some } 10^{12} \text{ cm}^{-4}$$

To achieve appreciable heating we have to apply additional power at a level of several times the Ohmic heating power. $P_{RF} \approx$ 2 MW is considered to be a reasonable amount for ASDEX to increase the plasma temperature by at least a factor of 2.

The major objective for ASDEX is to study the behaviour of impurities. Of interest is their behaviour on a long time scale especially when a large amount of rf-power is applied. The rf-pulse length should therefore exceed 1 sec.

3.) Discussion of frequency and $N_{\parallel}$-spectrum for ion heating by mode conversion

In this chapter we neglect effects due to toroidicity and those due to the poloidal magnetic field. Based upon the eqs. (2) and (4) we study accessibility and mode conversion for different frequencies, different $N_{\parallel}$-values, and various gas concentrations. For this purpose we plot the accessibility condition (2) and the mode conversion characteristics (4) as a function of the density and magnetic field. Figure 2 shows as an example the accessibility boundary in a hydrogen plasma for a wave with f = 1300 MHz and various values of $N_{\parallel}$. Because of the radial variation of the main magnetic field we also show a density profile in this figure, which is assumed to be parabolic. A lower hybrid wave with $N_{\parallel} = 1.75$, which in the case of fig. 2 propagates from the edge of the plasma towards the center, would only reach a radius $r \approx 25$ cm and is then reflected towards the plasma edge in the form of a fast wave. Only waves with $N_{\parallel} \gtrsim 1.8$

could in this case reach the plasma center. Increasing plasma density thus requires a larger $N_{\parallel}$ to satisfy the accessibility condition.

The dependence of the accessibility upon frequency is shown in fig.3. With increasing frequency the lower hybrid density increases as well, however the accessibility boundaries are shifted to lower densities. Therefore, to heat a plasma with higher density, we need a higher frequency and also a higher $N_{\parallel}$.

Figure 4 shows the dependence of the accessibility upon the relative hydrogen and deuterium concentrations. With increasing deuterium concentration the lower hybrid density increases, however, for accessibility we again need a higher $N_{\parallel}$.

Next we consider the mode conversion characteristics (eq. 4), as shown in fig. 5. They lie below the curve for the cold plasma lower hybrid density, their exact position depending upon the product $N_{\parallel}\sqrt{T_i}$. For given density and temperature profiles, and for a given $N_{\parallel}$-spectrum we can determine the locations in the plasma where mode conversion takes place and thus where the ions are heated. The waves with the lower values of $N_{\parallel}$ out of a spectrum penetrate deeper into the plasma. For a given $N_{\parallel}$-spectrum within the limits $N_{\parallel 1} < N_{\parallel} < N_{\parallel 2}$,

we can - with this kind of figures - determine the peak plasma density for which the low $N_{\parallel}$ edge of the spectrum ($N_{\parallel} = N_{\parallel 1}$) becomes absorbed in the center of the plasma. In table 1 we list these peak densities for different frequencies, different hydrogen-deuterium concentrations, different temperatures and $N_{\parallel}$-spectra. The values in brackets cannot be reached because (in this plane geometry approximation) the accessibility condition is violated. We see from this table that for $N_{\parallel 1} = 2.5$ and a frequency of 1100 MHz we can cover a density range of $3 \cdot 10^{13} \lesssim n_e(0) \lesssim 10^{14}$ cm^{-3} by varying the hydrogen-deuterium concentrations. At a frequency of f = 1300 MHz this density range is $5 \cdot 10^{13} \lesssim n_e(0) \lesssim 10^{14}$ cm^{-3}. Densities above $\approx 10^{14}$ cm^{-3} can not be reached with $N_{\parallel 1} = 2.5$ because of the accessibility condition.

These density ranges are of course only valid for waves with $N_{\parallel} \approx N_{\parallel 1}$, i.e. the low $N_{\parallel}$ part of the spectrum. Because of the finite width of the $N_{\parallel}$-spectrum the operational density range is in fact broader, however, at the expense of absorbable power.

The density range could be increased for spectra with a higher value of $N_{\parallel 1}$, like the case $N_{\parallel 1} = 3$ in table 1. However, in this case the dimensions of the coupler become smaller and thus the power density at the coupler increases.

$N_{\parallel min}$	$T_i(o)$[keV]	f [MHz]	H_2	50%H_2/50%D_2	25%H_2/75%D_2	D_2
		1100	3.6	5.6	(8.0)	(13.5)
	0.5	1200	4.6	(7.6)	(11.5)	(22)
		1300	6.1	(10.8)	(18.0)	(40)
		1100	3.4	5.2	7.3	(12.0)
2.0	0.7	1200	4.4	7.0	(10.3)	(20)
		1300	5.6	(9.8)	(16)	(32)
z.B.		1100	3.2	4.9	6.6	(11.4)
$2 < N_{\parallel} < 3.5$	1.0	1200	4.1	6.6	(9.7)	(17.5)
		1300	5.4	(9.3)	(14)	(28)
		1100	3.4	5.3	7.2	(12)
	0.5	1200	4.3	6.9	10.0	(18)
		1300	5.5	9.7	(15.5)	(30)
		1100	3.1	4.7	6.5	10.6
2.5	0.7	1200	4.0	6.4	9.3	(17)
		1300	5.2	8.8	(13.5)	(27)
z.B.		1100	2.9	4.4	6.0	9.8
$2.5 < N_{\parallel} < 4$	1.0	1200	3.7	5.8	8.5	(14.5)
		1300	4.9	8.2	(12)	(22)
		1100	3.1	4.8	6.5	10.5
	0.5	1200	4.0	6.4	9.2	17.0
		1300	5.1	8.9	(13.5)	(27)
		1100	2.9	4.4	6.0	9.5
3.0	0.7	1200	3.8	5.9	8.4	15
		1300	4.8	8.2	(12)	(23)
		1100	2.7	4.0	5.5	8.5
z.B.	1.0	1200	3.4	5.2	7.5	12.5
$3 < N_{\parallel} < 4.5$		1300	4.4	7.2	10.5	(19)

Table 1: Peak plasma densities n_e (0) in 10^{-13} cm^{-3} for which the linear turning point lies in the center region. B_o (0) = 25 kG.

In fig. 5 the parameters of the mode conversion characteristics is $N_{\parallel}\sqrt{T}$ and so this figure can be used for any temperature profile. In fig. 6 we assume a given central ion temperature and a parabolic squared temperature profile and arrive at mode conversion characteristics with only $N_{\parallel}$ as parameter. We now see that for a coupler spectrum $2.5 < N_{\parallel} < 4.0$ we heat in the center third of the plasma. Figure 7 shows a similar plot where we have used density and temperature profiles as obtained from the BALDUR transport code for ASDEX parameters.

These considerations are valid for an Ohmic target plasma with fixed parameters. When heating takes place the temperature rises and the temperature profile may change. This has the effect that the absorption zone, i.e. the mode conversion layer, shifts radially outward. However, for a temperature increase by a factor of 2 at a constant density and with constant profiles, the absorption zone remains within the center half of the plasma. This is also true for heating simulation calculations performed with the BALDUR-code, where profile modifications are allowed /14/.

The width of the $N_{\parallel}$-spectrum, $N_{\parallel 1} < N_{\parallel} < N_{\parallel 2}$, determines directly the width of the absorption region and should therefore not be too large. It is given by the dimensions of the coupler.

4.) Discussion of frequency and $N_{\parallel}$-spectrum for electron heating through electron Landau damping

In the previous chapter we discussed the ion heating which occurs in that region of the plasma, where the incident lower hybrid wave is converted into an electrostatic ion Bernstein wave. However, if the wave refractive index component $N_{\parallel}$ is large enough, the electrons also contribute to the damping of the lower hybrid waves through electron Landau damping parallel to the magnetic field. According to quasilinear theory this damping becomes appreciable if, /7/:

$$N_{\parallel}\sqrt{T_e\,[keV]} \approx 6.4 \qquad (5)$$

As a consequence it is possible for large enough $N_{\parallel}$'s, or in a plasma with a high electron temperature, that the wave is damped by the electrons before it can reach the mode conversion layer.

The electron- or ion heating regimes with respect to density and temperature /7/ are shown in figs. 8a and b, where we assumed $T_e = T_i$. In these figures, valid for fixed frequency, magnetic field and gas concentration, the solid lines represent the mode conversion characteristics (eq. 4) and the thin dashed lines are the characteristics for electron Landau damping (eq. 5). Dis-

regarding the inhomogeneity of the magnetic field in these plots, we can trace a lower hybrid wave penetrating from the plasma edge towards the plasma center at higher density and higher temperature, as sketched in fig. 8a. In the first example we assume a peak plasma density of $n_e(0) \approx 9 \cdot 10^{13}$ cm^{-3} and a peak temperature of $T_i(0) \approx 700$ eV, in which case a wave with $N_{\parallel} \approx 3$ would be absorbed near the center through mode conversion leading mainly to ion heating. In the second example sketched, we assume a much lower central density, $n_e(0) \approx 3 \cdot 10^{13}$ cm^{-3} and $T_e(0) \approx 1$ kV. In this case a wave with $N_{\parallel} \approx 6$ would be absorbed near the center of the plasma through electron Landau damping, leading mainly to electron heating. There is a density limit above which ion heating through mode conversion occurs, and below which electron heating through Landau damping is dominant. This density limit depends, as obvious from figs. 8, upon the hydrogen-deuterium concentration, but not upon $N_{\parallel}$ and the temperature. With increasing frequency this density limit shifts to higher values. Table 2 shows the values of the density in units of 10^{13} cm^{-3} in this transition region for different frequencies and hydrogen-deuterium concentrations at a fixed magnetic field of 25 kG.

From figs. 8 we also recognize that at temperatures above some keV the mode conversion regime becomes very narrow and that operation in the transition area to the electron Landau damping regime becomes increasingly important.

Table 2:

f , MHz	H_2	50 % Hz/50 % D_2	D_2
1100	1.8	2.5	4.7
1200	2.25	3.2	6.4
1300	2.8	4.0	8.6
1400	3.4	5.1	12.0
1500	4.2	6.6	17.3

5.) Choice of frequency and $N_{||}$-spectrum for the ASDEX lower hybrid experiment

As seen in the previous chapters, ion heating in the mode conversion regime can be achieved in ASDEX over a fairly broad frequency range, however for higher frequencies the possible density range becomes narrower. On the other hand, for electron heating through Landau damping, we have to choose the frequency high enough to be able to heat at reasonable densities for ASDEX.

With the choice of 1300 MHz for the ASDEX lower hybrid experiment we can work in both heating regimes. For ion heating of an Ohmic target plasma we need a coupler with an

average $N_{\parallel}$ of $\langle N_{\parallel} \rangle \approx 3$, and for electron heating a coupler with $\langle N_{\parallel} \rangle \approx 6$ is necessary. The width of the $N_{\parallel}$-spectrum, $\Delta N = N_{\parallel 2} - N_{\parallel 1}$, should in both cases not exceed 1.5 in order to obtain a reasonable centered power deposition profile. These values are the result of applying the plane wave equations and neglecting the poloidal magnetic field.

Ray tracing calculations, taking these effects into account as well as realistic density and temperature profiles for ASDEX, corroborate the choice of $\langle N_{\parallel} \rangle = 3$ for the ion heating experiment. These results are shown in fig. 9 which shows the fate of a wave starting at the plasma boundary at r = a (in the major plane of the torus) with a $N_{\parallel} = N_{\parallel}(a)$. Waves with $N_{\parallel}(a) \lesssim 2.3$ are at the accessibility boundary converted into a fast electromagnetic wave and return to the plasma edge. Waves with $N_{\parallel}(a) \gtrsim 2.3$ experience mode conversion well inside the plasma.

6.) The coupler

The purpose of the coupler is to launch waves with a $N_{\parallel}$-spectrum as is necessary to meet the accessibility condition and also to match the plasma impedance to the wave impedance of the transmission line. These requirements can be met with a "grill"-coupler /8/ consisting

of a phased array of reduced height waveguides with their electric field oriented parallel to the toroidal magnetic field. Figure 10 shows a schematic of the grill foreseen for the ASDEX ion heating experiment. If the fields in adjacent waveguides are out of phase, we can approximate the total electric field distribution in front of the grill by the functional

$$f(x) = f_1(x) \cdot f_2(x) \tag{6}$$

where $f_1(x)$ is a square wave function, corresponding to the field periodicity of the grill, and $f_2(x)$ is an envelope function, describing the length of the coupler and the relative amplitudes in the individual waveguides (fig. 11). The exciting wavenumber spectrum then is

$$F(k) = F_1(k) * F_2(k). \tag{7}$$

The square wave function $f_1(x)$ in fig. 11 can be written as an infinite sum of sine-functions. The Fourier transform $F_1(k)$ thus is a line spectrum with lines at $k = k_n = (2n-1)\frac{2\pi}{a}$, a being the periodicity length of the grill. For the case of fig. 11, i.e. equal amplitudes in all waveguides, the convolution product, eq. (7), then yields:

$$F(k) = -i\,\frac{2}{\pi}\sum_{n=1}^{\infty}\frac{1}{2n-1}\left\{F_2(k-k_n) - F_2(k+k_n)\right\}. \tag{8}$$

This is again a line spectrum corresponding to $F_1(k)$, however each line now shows a profile which corresponds to the Fourier transform $F_2(k)$ of the envelope function $f_2(x)$, and thus depends on the total length of the grill. For our lower hybrid heating purpose, the first line only is of importance and yields the coupler spectrum. Figure 12 shows this coupler spectrum $F(k) \cdot F^*(k)$ of an 8 waveguide grill for two different values of a.

For the values of $\langle N_{\parallel} \rangle = k_1 \, c/\omega = \lambda_0/a$ which we want to realize in ASDEX according to chapter 5 and for f = 1300 MHz we obtain for a the values listed in table 3. Also listed are the values of $\Delta N_{\parallel}$ for grills with different numbers of waveguides.

Table 3:

$\langle N_{\parallel} \rangle$	a [mm]	$\Delta N_{\parallel}$			
		number of waveguides			
		6	8	12	16
2.75	84	1.83	1.38		
3.00	77	2.00	1.50		
3.25	71	2.17	1.63		
3.50	66	2.33	1.75		
5.5	42.0		2.76	1.83	1.38
6.0	38.5		3.00	2.00	1.50
6.5	35.5		3.26	2.17	1.63
7.0	33.0		3.50	2.33	1.75

From this table we recognize, that a grill for ion heating with $\langle N_{\parallel} \rangle \simeq 3.0$ should at least have 8 waveguides to produce a spectrum with $\Delta N_{\parallel} \approx 1.5$. The grill for the electron heating with $\langle N_{\parallel} \rangle \approx 6$ should, for the same reason, consist of about 16 waveguides, i.e. its total length will then be about the same as that of the ion heating grill. The requirements for a grill for a plasma current drive experiment in an ohmically heated target plasma are similar to the one for electron heating, i.e. $\langle N_{\parallel} \rangle \simeq 6$. However, since this requires a relative phasing of $\Delta\varphi = \pi/2$, the number of waveguides must be further increased to about 32, each waveguide having half the height of those of the electron heating grill.

The linear theory of such couplers is well known for the case k_Θ = 0, /9, 10, 11, 12/. We used the code of M. Brambilla to study the behaviour of the ASDEX grill with respect to the phases and the amplitudes in the individual waveguides, as well as with respect to its dimensions. In figs. 13 we show, for two examples of the $\langle N_{\parallel} \rangle$ = 3 grill, the power reflection coefficients R_n in each waveguide and the average power reflection coefficient $\langle R \rangle$ for the whole grill. The quantity Q, as defined by H. Pacher /12/, is inversely proportional to the maximum power which can be transmitted with the grill for a given limiting rf-voltage in the waveguides.

It has been calculated neglecting waveguide cutoff modes. The corresponding power spectrum is shown in fig. 14. We see that an average power reflection coefficient $\langle R \rangle \lesssim 10$ % can be achieved, i.e. the grill is well matched to the plasma, thus requiring no special tuning to match the transmission line impedance. The minimum of $\langle R \rangle$ with respect to the density gradient is rather broad (one order of magnitude) and is located at $\nabla n \approx 10^{12}$ cm^{-4}, a gradient which we expect in the experiment.

For the $\langle N_n \rangle \approx 6$ grill for electron heating, the minimum of $\langle R \rangle$ occurs at a larger density gradient, $\nabla n \approx 10^{13}$ cm^{-4}, because of the shorter evanescene length of the lower hybrid waves in the cutoff region in front of the grill.

Reflection coefficient, power spectrum, and maximum transmittable power vary somewhat if the amplitudes in the individual waveguides are changed. Optimization is possible in two directions. First, the power in the non-accessible part of the spectrum should be a minimum. In the example of fig. 13a this part of the power is $\lesssim 3$ %, at a Q-value of 2.7. A second way to optimize is with respect to Q, i.e. to maximize the transmittable power, which increases the smaller Q is. In the example of fig. 13b, $Q \approx 2{,}0$, however the power in the non-accessible part of the spectrum is ≈ 9 %. The power

handling capability of the grill is considerably higher than in the case of fig. 13a, however the power in the non-accessible waves increases as well, which may lead to surface heating. The experiment will have to show whether this can be tolerated.

The computer code of M. Brambilla also includes waveguide cutoff modes. Their influence is mainly upon the radiated power spectrum due to the enhancement of the electric field at the grill edges, which results in a stronger excitation of very short wavelength plasma waves (lines k_2 and k_3 in fig. 11). The code, however, can only treat the case of sharp edges. With rounded corners we expect that these cutoff modes are much less excited, since their 1/e-evanescence lengths are $\lesssim 10$ mm. In fig. 15 we see the dependence of the average power reflection coefficient, the quality factor Q and the power in the useful spectral range upon the wall thickness d, keeping the periodicity length of the grill (b+d) constant. We see in fig. 15a that the useful power increases with increasing wall thickness, while the amplitudes of the reflected waveguide cutoff modes decrease, fig. 15b. However, increasing wall thickness leads to a higher power density in the waveguides, which should be kept low. For the ASDEX ion heating grill with $\langle N_{\parallel} \rangle = 3$ we choose, as a compromise, d = 8 mm for the wall thickness. Thus, the ion heating grill for ASDEX

will consist of an array of 8 waveguides with interior dimensions a x b = 165 x 30 mm, with a wall thickness of d = 8 mm between the waveguides. Figure 10 shows a sketch of this grill.

Acknowledgement

Many discussions with the members of the high frequency heating project of the IPP and the members of the WEGA-team in Grenoble led to the final choice of parameters and are gratefully acknowledged. Special thanks are for Dr. M. Brambilla who gave us his grill code and who run his ray tracing code for our parameters.

References

/1/ Brambilla,M., "The theory of lower hybrid heating of tokamak plasmas"
Proc. Conf. on Heating in Toroidal Plasmas
Grenoble 1978, Bd. II, S. 251

/2/ Bers, A., "The theory of plasma heating in the lower hybrid range of frequencies."
3rd topical conf. on rf-plasma heating,
Calif. Inst. of Techn., Pasadena, 1978, paper A-1

/3/ Golant, V.E., "Plasma penetration near the lower hybrid frequency."
Sov. Phys. Tech. Phys. 16 (1972), 1980

/4/ Lallia, P., "Location of the lower hybrid heating absorption zone in toroidal plasmas."
Report EUR-CEA-FC-774 (1975)

/5/ Fedorov, V.I., "The Theory of Lower Hybrid Heating in Tokamaks."
3rd Int.Symp. on Heating in Toroidal Plasmas,
Como, Sept. 1980

/6/ Brambilla, M., "Ray tracing of lower hybrid waves in toroidal plasmas",
3rd Int.Symp. on Heating in Toroidal Plasmas,
Como, Sept. 1980

/7/ Tonon, G., et al., in Commission of European Communities
Report EUR-FU-BRU XII/487/80

/8/ Lallia, P., Proc. 2nd Topical Conf. on RF-Plasma Heating, Lubbock 1974, paper C 3

/9/ Brambilla, M., "Waveguide launching of lower hybrid waves"
Nucl. Fusion 19 (1979), 1343 and
Nucl. Fusion 16 (1976), 47

/10/ Leuterer, F., Derfler, H.: "On the mutual interaction of rf-coupling gaps"
Plasma Physics 19 (1977), 539

/11/ Krapchev, V., Bers, A.: "Waveguide array excitation of lower hybrid fields in a Tokamak plasma"
Nucl. Fusion 18 (1978), 519

/12/ Pacher, H.: "Optimization of power spectra of multiwaveguide grills"
IPP-Report 2/247, Dez. 1979

/13/ Brambilla, M.: "Power deposition profiles during lower hybrid heating of Tokamak plasmas"
Inst. f. Plasmaphysik, Report IPP 4/200

/14/ Eckhartt, D., McKenney, A.: "Transport code predictions on the performance of lower hybrid heating in the ASDEX tokamak"
IPP-Report 4/197, March 1981

Figures:

1) Qualitative dispersion characteristics for electromagnetic waves in an inhomogeneous plasma near $\omega = \omega_{LH}$

——— real part, ----- imaginary part

n_{ACC} = density limit for penetration according to eq. (2)

n_{LH} = density at the cold plasma lower hybrid resonance

n_{LTP} = density at the linear turning point according to eq. (4).

a) $0 < N_{\parallel} < 1$; b) $1 < N_{\parallel} < N_{\parallel crit}$;

c) $N_{\parallel crit} < N_{\parallel}$

2) Accessibility boundary, eq. (2), as a function of density and magnetic field. Dashed lines: parabolic density profile for ASDEX dimensions

3) Frequency dependence of the lower hybrid density and the accessibility boundary

4) Dependence of the lower hybrid density and the accessibility boundary on the H_2-D_2-concentration

5) Mode conversion characteristics, $N_{\parallel} \sqrt{T}$ = const, and accessibility boundary. (T in keV)

a) in 100 % H_2

b) in 50 % H_2 + 50 % D_2

c) in 100 % D_2

6) Mode conversion characteristics ($N_{\parallel}$ = const) in a plasma with ASDEX dimensions, with a parabolic density profile and a parabolic squared temperature profile

7) Mode conversion characteristics ($N_{\parallel}$ = const) in an ASDEX plasma with profiles as obtained from the BALDUR code

8) Mode conversion - and electron Landau damping regions in a density - temperature diagram

—..— mode conversion characteristics ($N_{\parallel}$ = const), eq. (4)

----- characteristics for electron Landau damping $N_{\parallel}$ = const), eq. (5)

a) in 50 % H_2 + 50 % D_2

b) in 100 % D_2

9) Penetration of lower hybrid waves into an ASDEX plasma, as obtained through ray tracing calculations. $N_{\parallel}(a)$ is the value of $N_{\parallel}$ at the plasma boundary. The profiles of $n_e(r)$, $T_{e,i}(r)$ and $q(r)$ are taken from BALDUR-code calculations. The thin dashed lines represent the $N_{\parallel}$-spectrum of the ion heating grill with $\langle N_{\parallel} \rangle = 3$.

B_o = 2.5 T, $q(a) = 4$, f = 1.3 GHz, gas: H_2.

LTP: the wave experiences a linear turning point, according to eq. (4)

(9) WGR: the wave experiences a "whispering gallery regime"

CONFL: the lower hybrid wave experiences a confluence into a fast wave, according to eq. (2).

10) Sketch of the 8-waveguide grill as planned for ion heating in ASDEX

11) Field distribution and spectrum of an 8-waveguide grill

a) field distribution E(x)

b) square wave function $f_1(x)$

c) envelope function $f_2(x)$

d) spectrum F(k)

12) Coupler spectrum $E(k) \cdot E^*(k)$ of an 8 waveguide grill driven out of phase and with equal amplitudes

13) Power reflection coefficients ($R_1 = R_8$, $R_2 = R_7$, $R_3 = R_6$, $R_4 = R_5$) in the individual waveguides of an 8 waveguide grill, average reflection coefficient $\langle R \rangle$ of the total grill and grill quality Q (neglecting waveguide cutoff modes).

f = 1300 MHz, a = 76 mm, d = 8 mm

a) total electric field at the grill mouth

$E_1 = 0{,}46$; $E_2 = -1.0$; $E_3 = 1.22$;

$E_4 = 1.32$; $E_5 = -E_4$, $E_6 = -E_3$, $E_7 = -E_2$;

$E_8 = -E_1$;

(13) b) specified incident wave field

$E_1 = +1.0$; $E_2 = -1.0$; $E_3 = +1.0$;

$E_4 = -1.0$;

14) Power spectrum of the waves penetrating into the plasma for the case of fig. 13a at

$\nabla n = 10^{12}\ cm^{-4}$

15) Variation of the wall thickness at a constant periodicity length a = 76 mm of an 8 waveguide grill. Four waveguide cutoff modes are included in the calculation.

f = 1300 MHz; $\nabla n = 10^{12}\ cm^{-4}$;

total field in the grill mouth:

$E_1 = 0.58$; $E_2 = -1.0$; $E_3 = 1.3$; $E_4 = -1.3$.

a) power in the useful spectral range $P_{N_{\parallel}} = 2\ ./.\ 4$; average reflection coefficient $\langle R \rangle$ and quality Q.

b) amplitudes of the more important waves in the center waveguides.

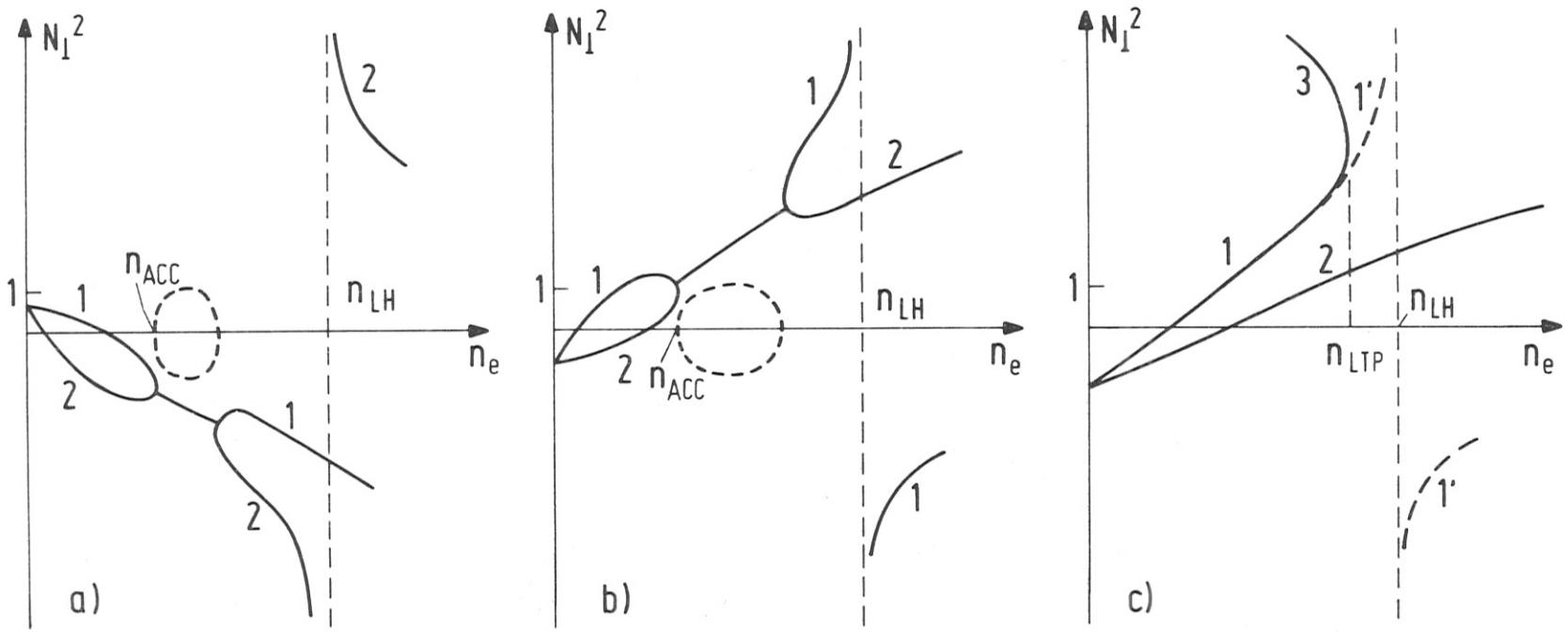

FIG. 1

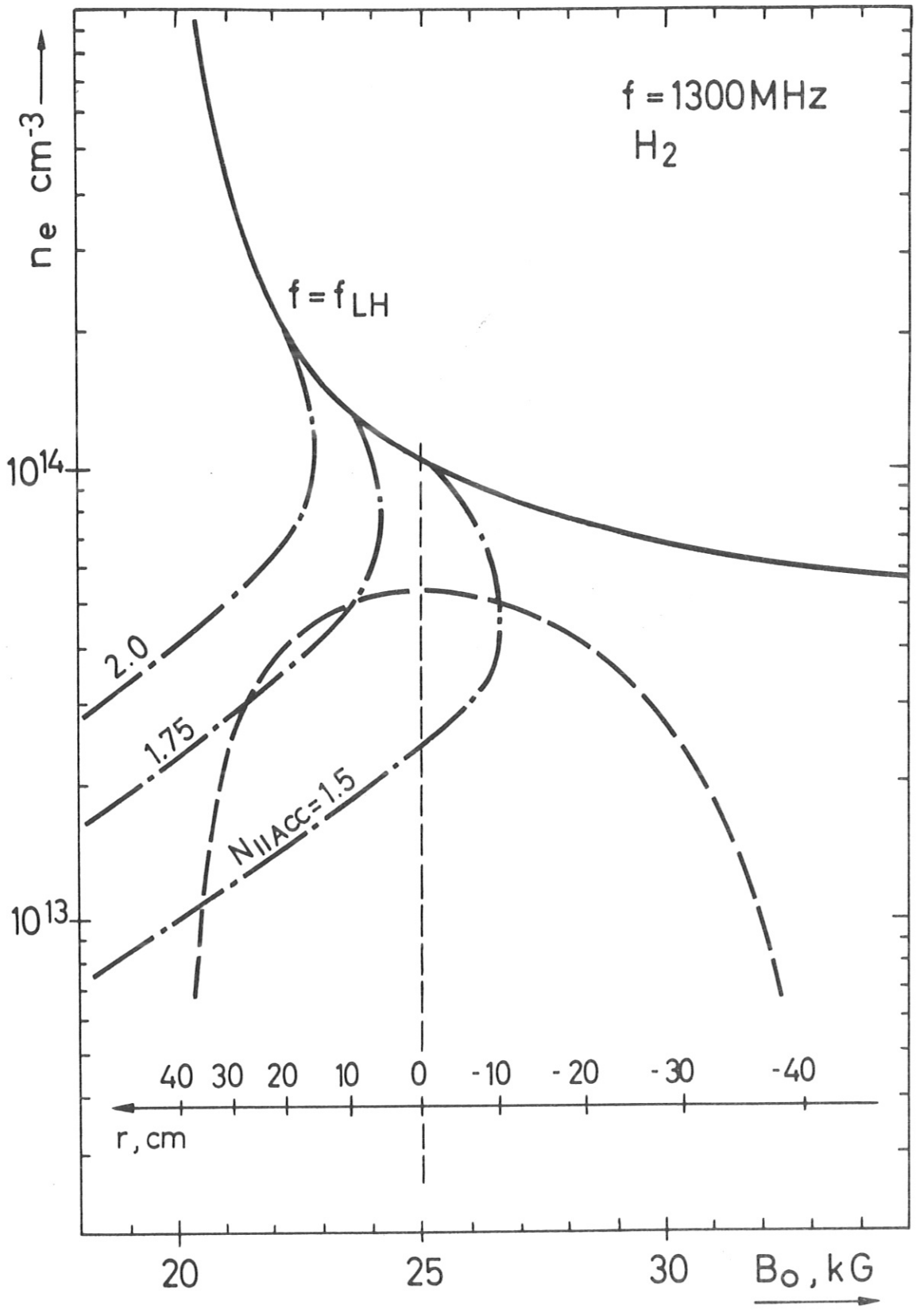
f = 1300 MHz
H2
f = fLH
ne cm-3
10^14
10^13
2.0
1.75
N||ACC=1.5
40 30 20 10 0 -10 -20 -30 -40
r, cm
20 25 30 Bo, kG

FIG. 2

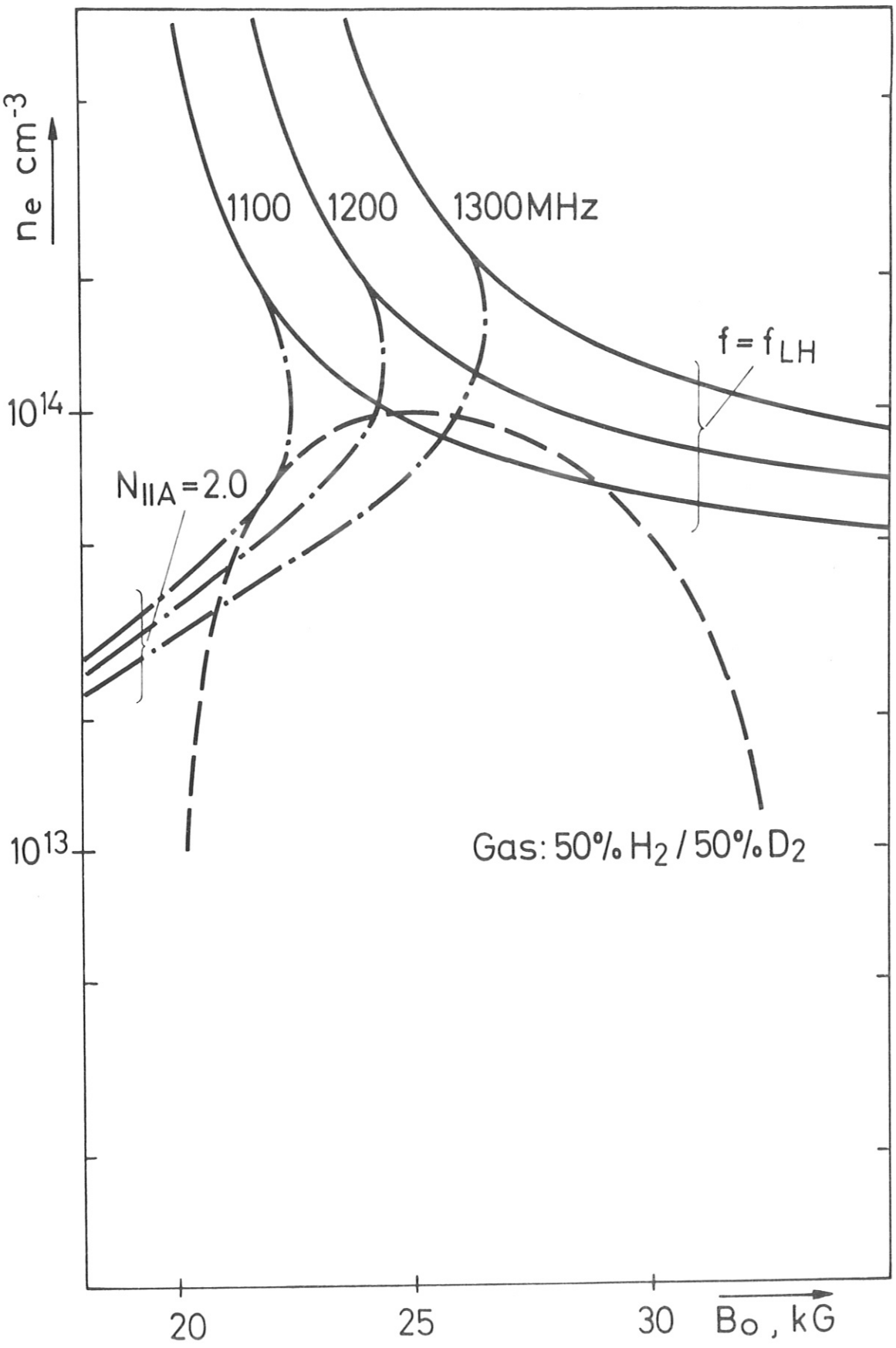
n_e cm^{-3}
1100
1200
1300MHz
$f = f_{LH}$
10^{14}
$N_{IIA} = 2.0$
10^{13}
Gas: 50% H_2 / 50% D_2
20
25
30
B_o, kG

FIG. 3

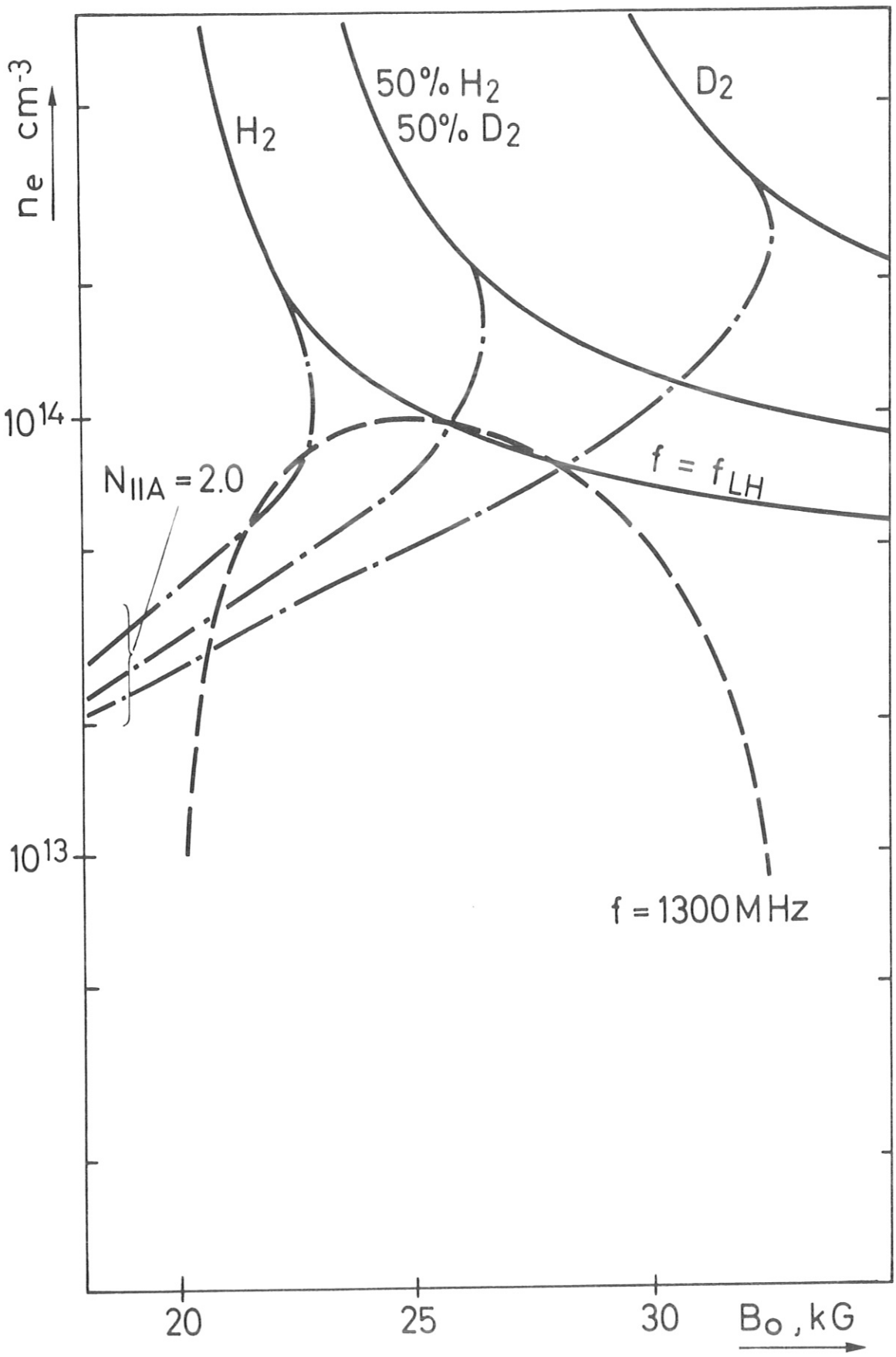
n_e cm^{-3}
10^{14}
10^{13}
H_2
50% H_2
50% D_2
D_2
$N_{IIA} = 2.0$
$f = f_{LH}$
f = 1300 MHz
20
25
30
B_o, kG

FIG. 4

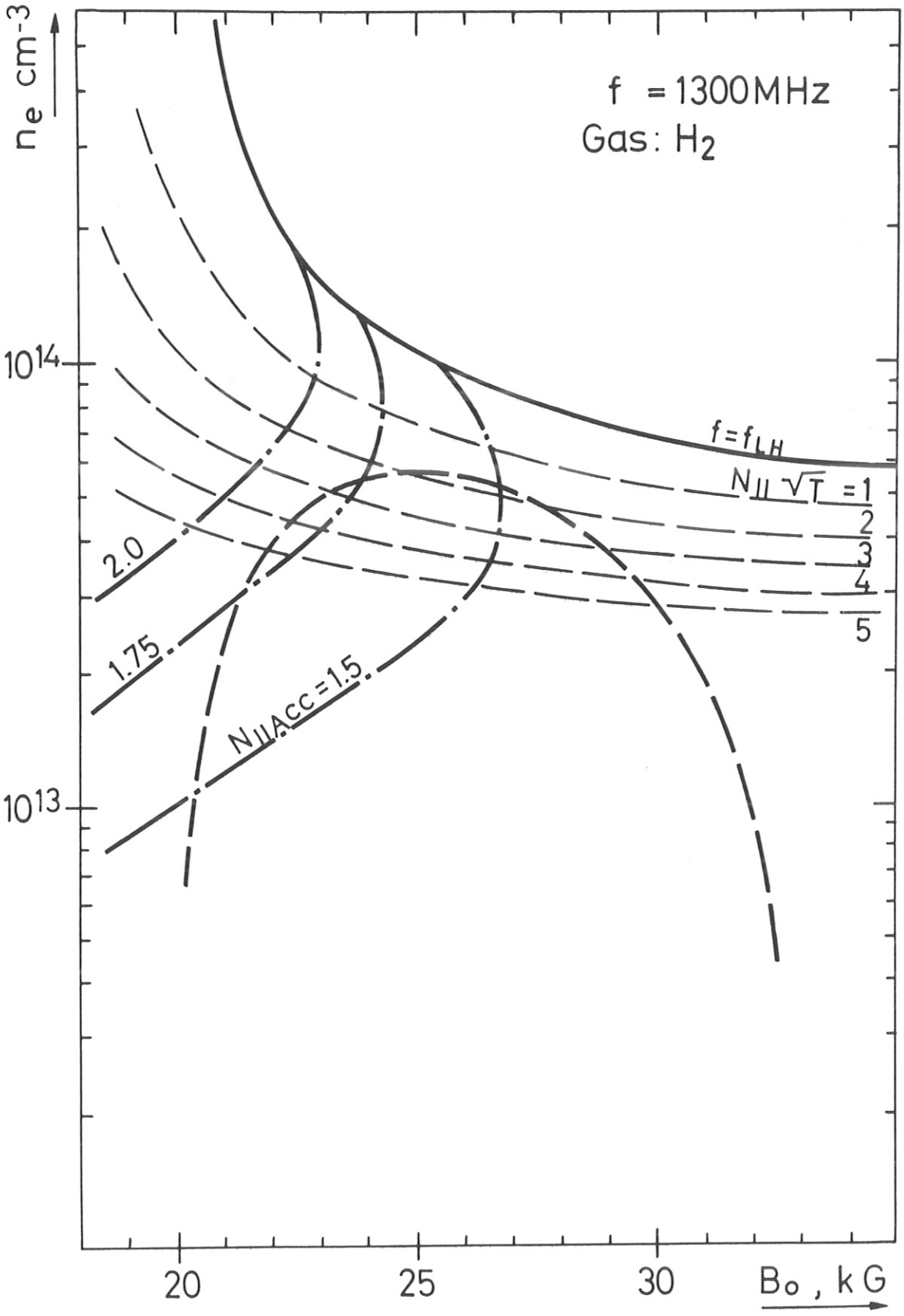
n_e cm^{-3}
10^{14}
10^{13}
f = 1300 MHz
Gas: H_2
$f = f_{LH}$
$N_{\parallel}\sqrt{T}$ = 1
2
3
4
5
2.0
1.75
$N_{\parallel ACC}$ = 1.5
20
25
30
B_o, kG

FIG. 5A

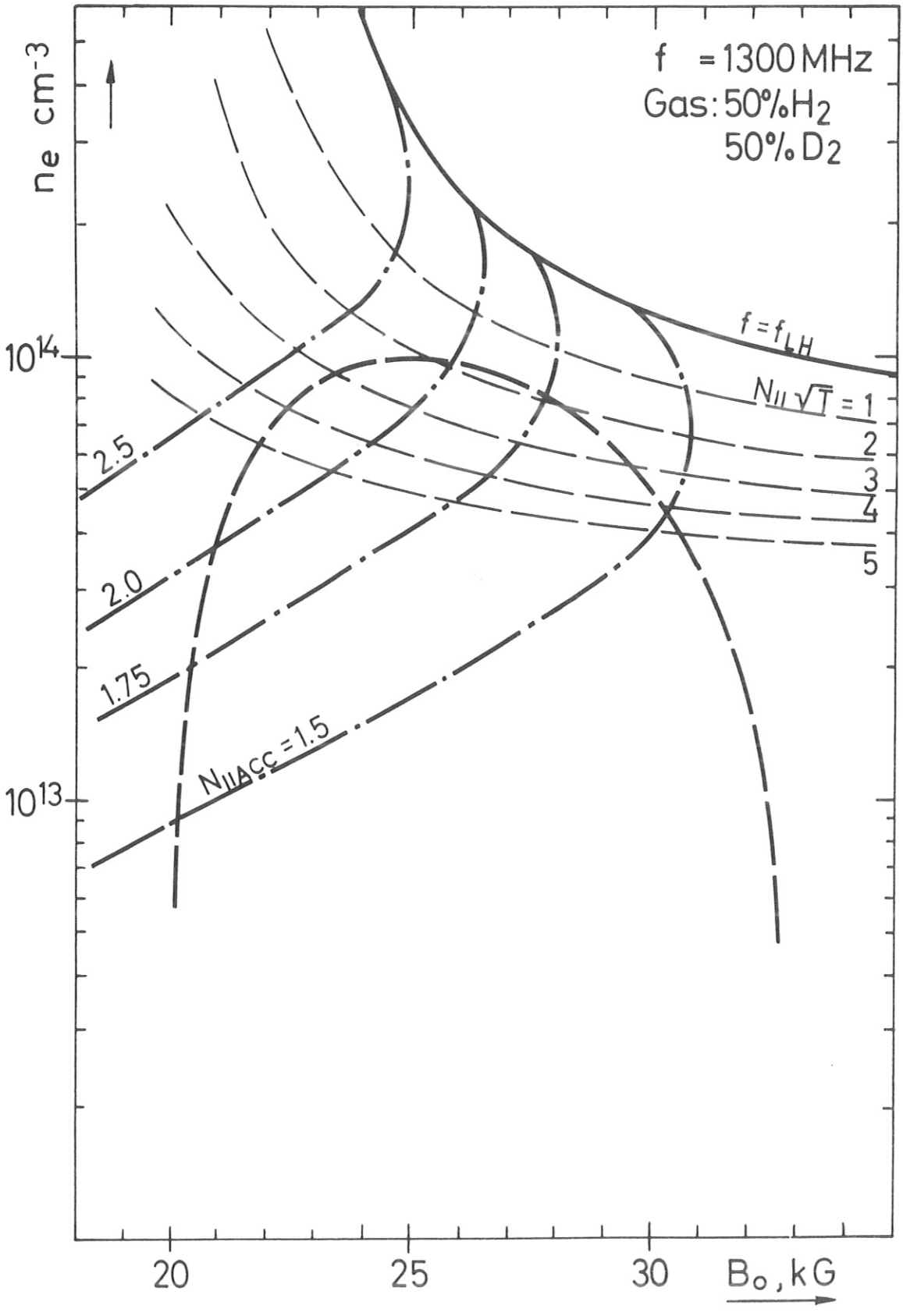
f = 1300 MHz
Gas: 50% H2
50% D2
ne cm-3
10^14
10^13
f = fLH
N∥√T = 1
2
3
4
5
2.5
2.0
1.75
N∥Acc = 1.5
20
25
30
Bo, kG

FIG. 5B

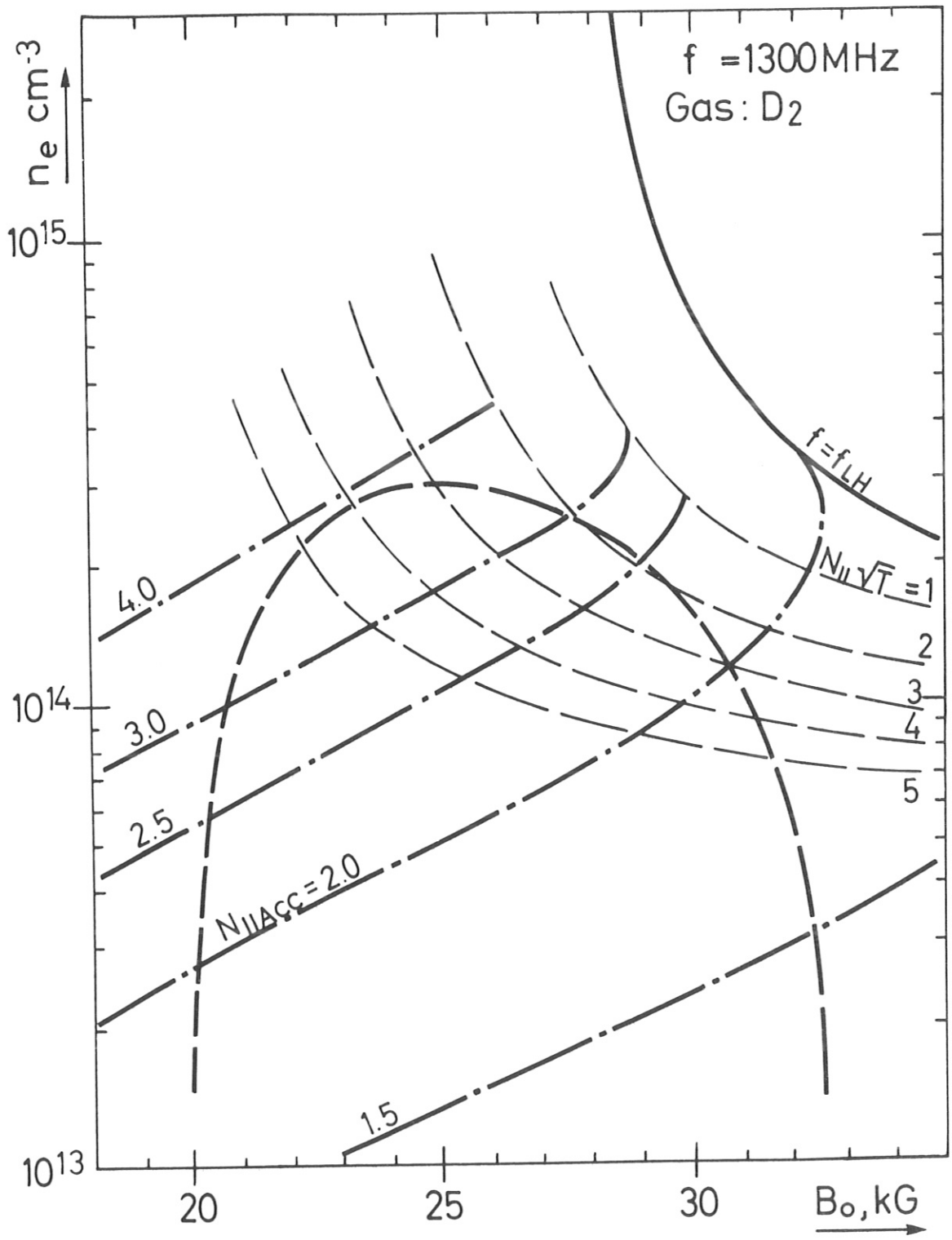
f =1300MHz
Gas: D2
ne cm-3
10^15
10^14
10^13
20
25
30
Bo, kG
f=fLH
N∥√T =1
2
3
4
5
4.0
3.0
2.5
N∥Acc=2.0
1.5

FIG. 5c

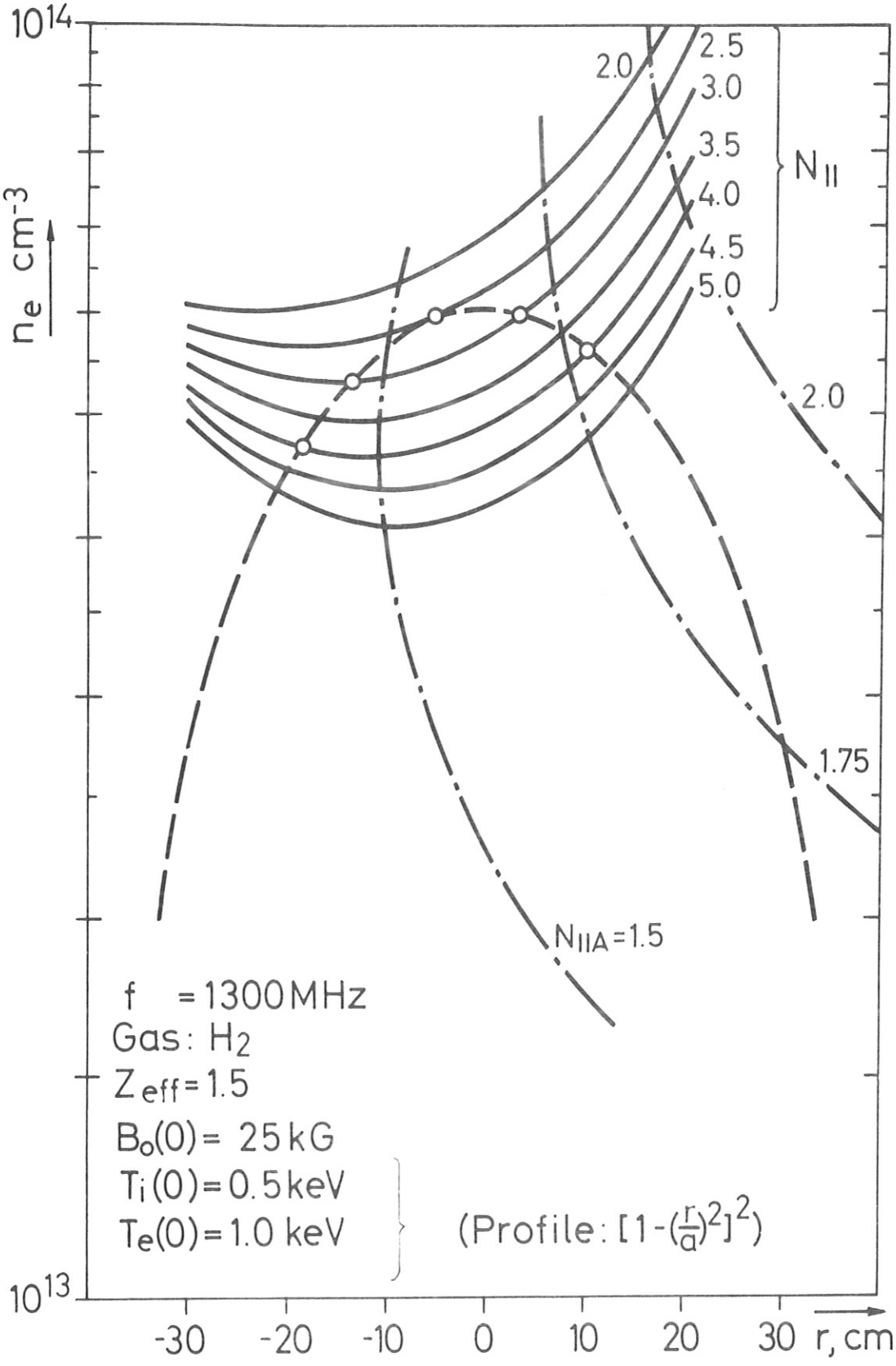
10^{14}
10^{13}
n_e cm^{-3}
2.0
2.5
3.0
3.5
4.0
4.5
5.0
N_{II}
2.0
1.75
N_{IIA}=1.5
f = 1300 MHz
Gas: H_2
Z_{eff} = 1.5
$B_o(0)$ = 25 kG
$T_i(0)$ = 0.5 keV
$T_e(0)$ = 1.0 keV
(Profile: $[1-(\frac{r}{a})^2]^2$)
-30
-20
-10
0
10
20
30
r, cm

FIG. 6

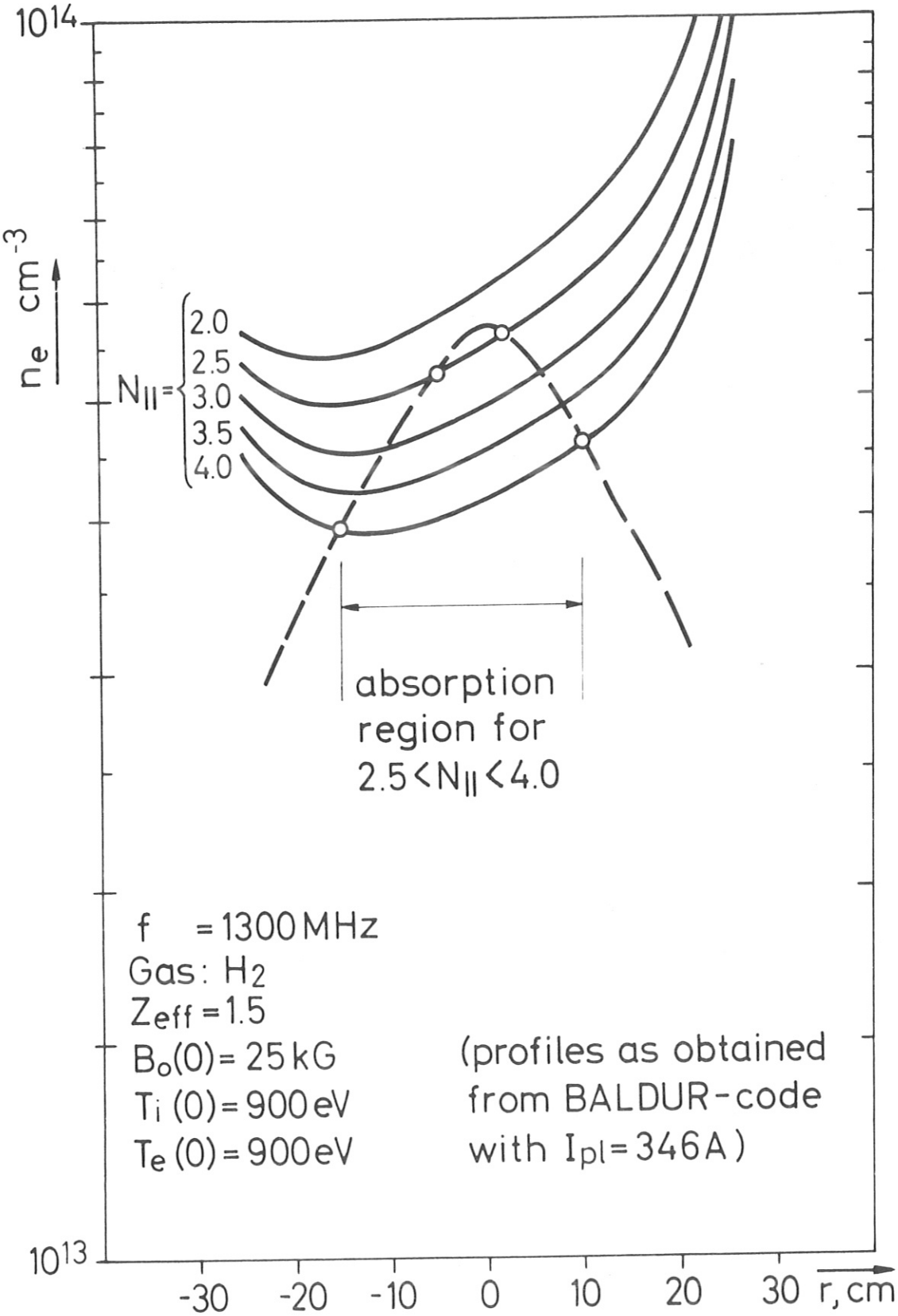
10^{14}
n_e cm^{-3}
$N_{||}$ = 2.0 2.5 3.0 3.5 4.0
absorption region for $2.5 < N_{||} < 4.0$
f = 1300 MHz
Gas: H_2
Z_{eff} = 1.5
$B_o(0)$ = 25 kG
$T_i(0)$ = 900 eV
$T_e(0)$ = 900 eV
(profiles as obtained from BALDUR-code with I_{pl} = 346 A)
10^{13}
-30 -20 -10 0 10 20 30 r, cm

FIG. 7

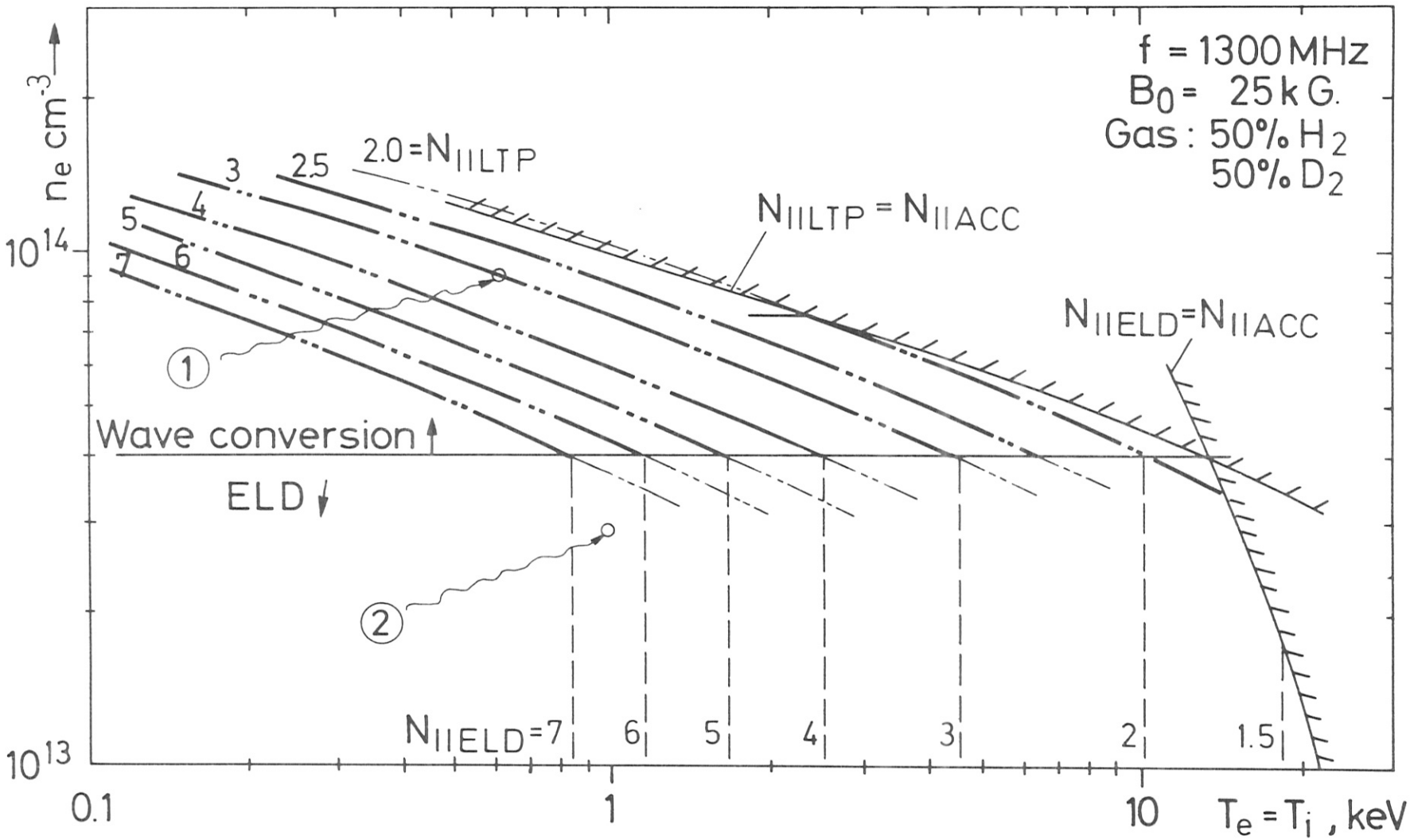
f = 1300 MHz
B0 = 25 k G.
Gas : 50% H2
50% D2
ne cm-3
10^14
10^13
2.0 = NIILTP
2.5
3
4
5
6
7
NIILTP = NIIACC
NIIELD = NIIACC
1
2
Wave conversion
ELD
NIIELD = 7
6
5
4
3
2
1.5
0.1
1
10
Te = Ti , keV

FIG. 8A

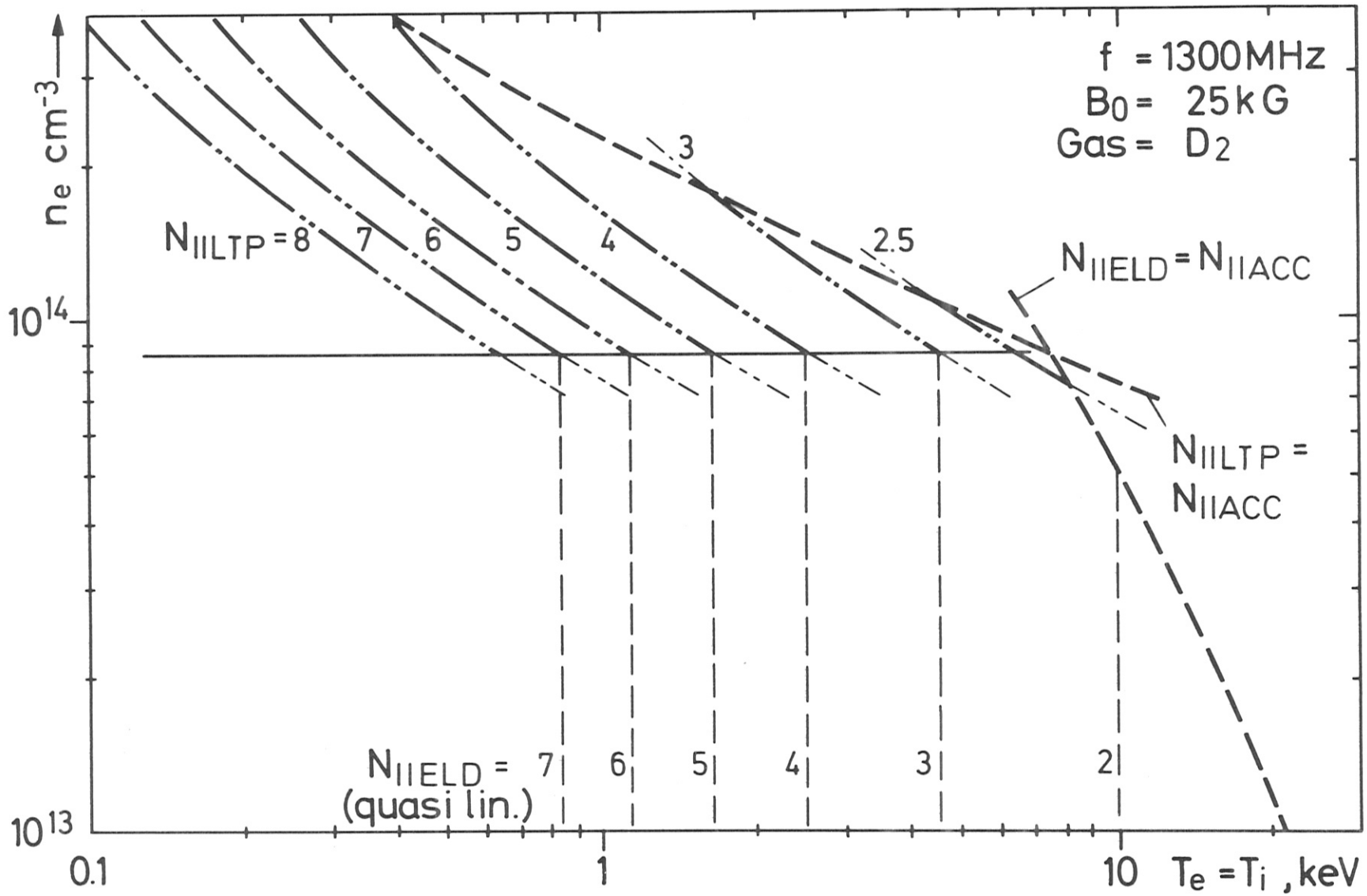
f = 1300MHz
B0 = 25kG
Gas = D2
ne cm-3
10^14
10^13
0.1
1
10
Te = Ti , keV
NIILTP = 8
7
6
5
4
3
2.5
NIIELD = NIIACC
NIILTP = NIIACC
NIIELD = (quasi lin.)
7
6
5
4
3
2

FIG. 8B

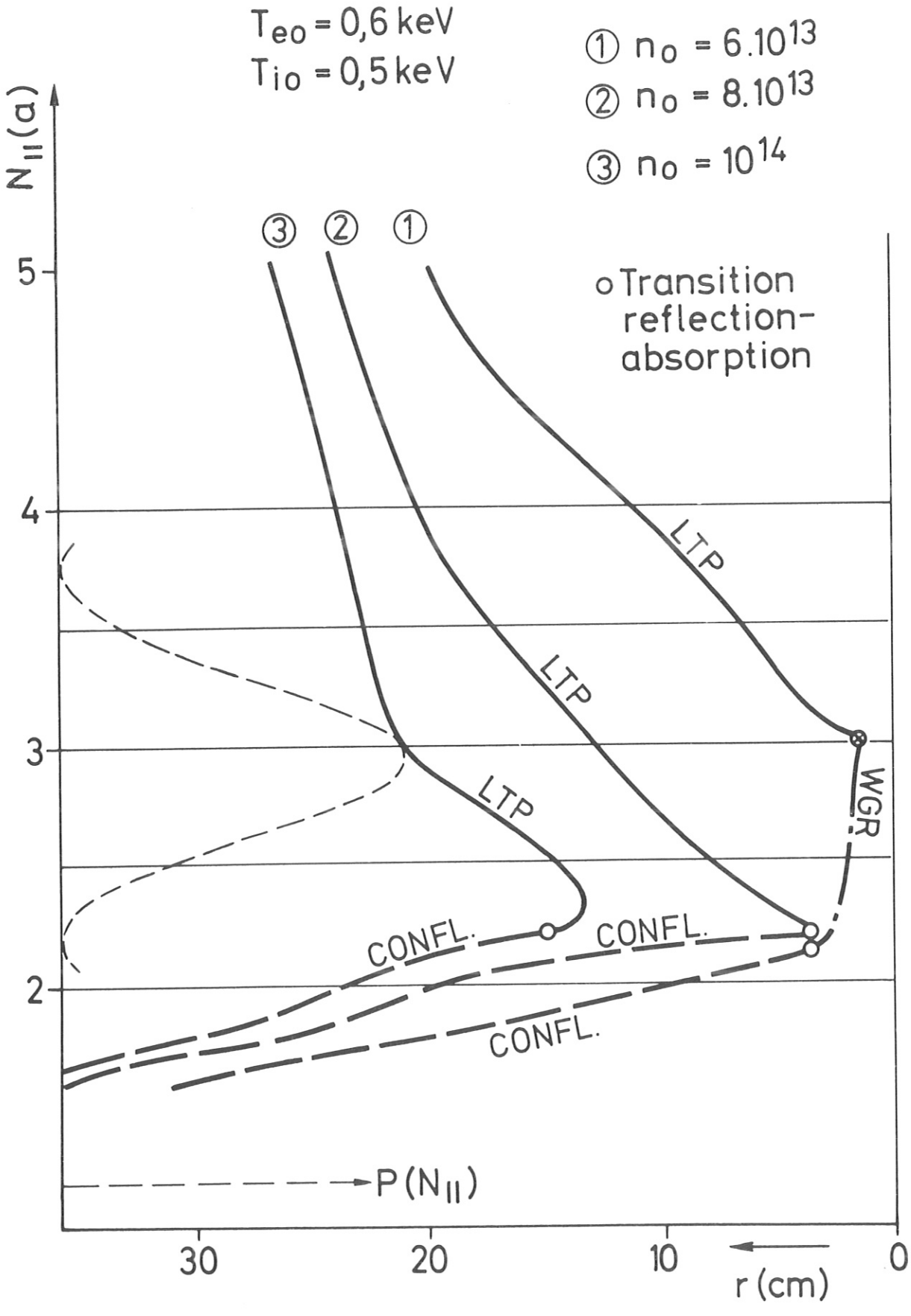
$T_{eo} = 0{,}6$ keV
$T_{io} = 0{,}5$ keV
① $n_o = 6.10^{13}$
② $n_o = 8.10^{13}$
③ $n_o = 10^{14}$
$N_{II}(a)$
5
4
3
2
o Transition reflection-absorption
LTP
LTP
LTP
WGR
CONFL.
CONFL.
CONFL.
$P(N_{II})$
30
20
10
0
r (cm)

FIG. 9

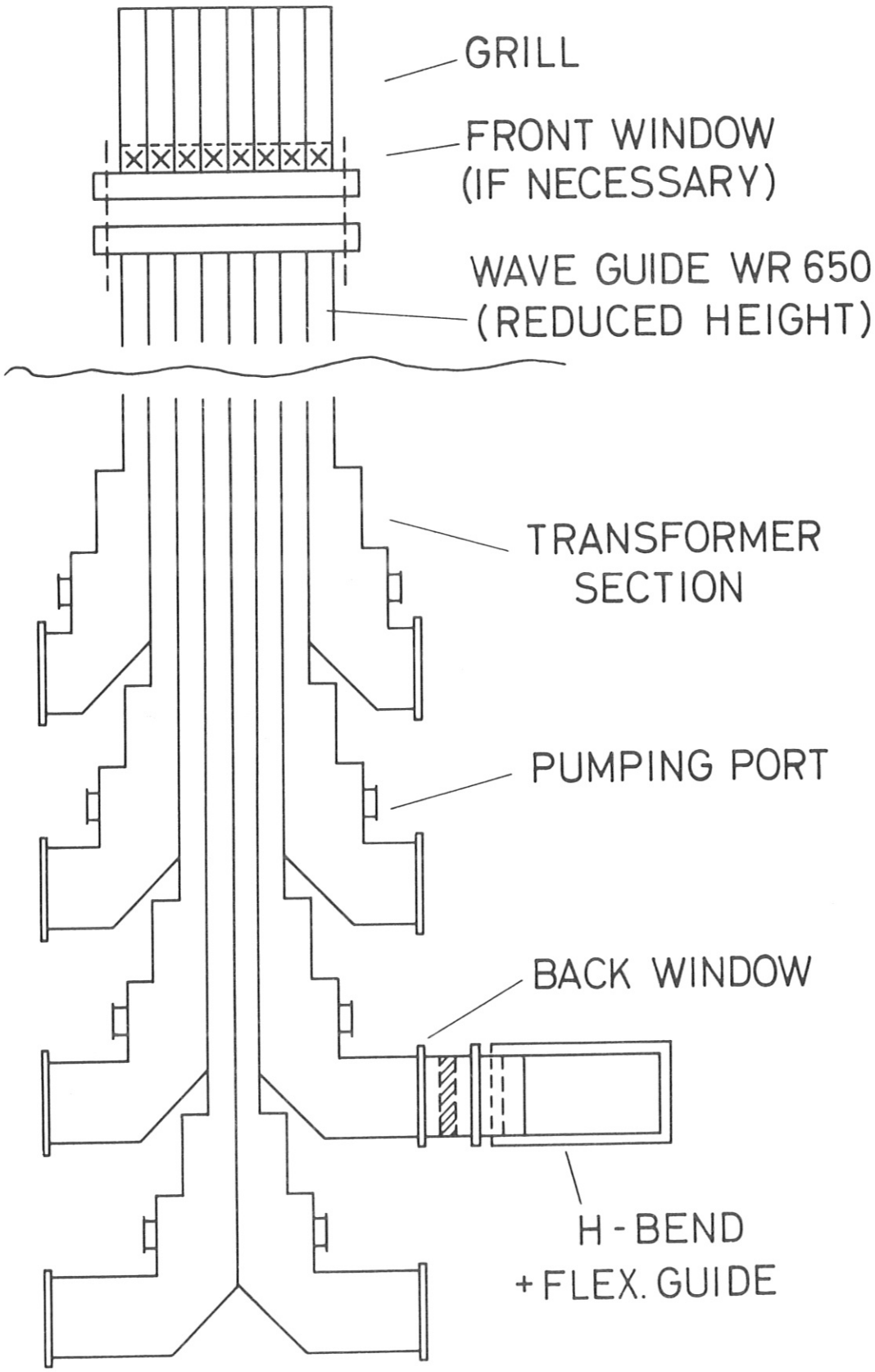
GRILL
FRONT WINDOW
(IF NECESSARY)
WAVE GUIDE WR 650
(REDUCED HEIGHT)
TRANSFORMER
SECTION
PUMPING PORT
BACK WINDOW
H-BEND
+FLEX. GUIDE

FIG.10

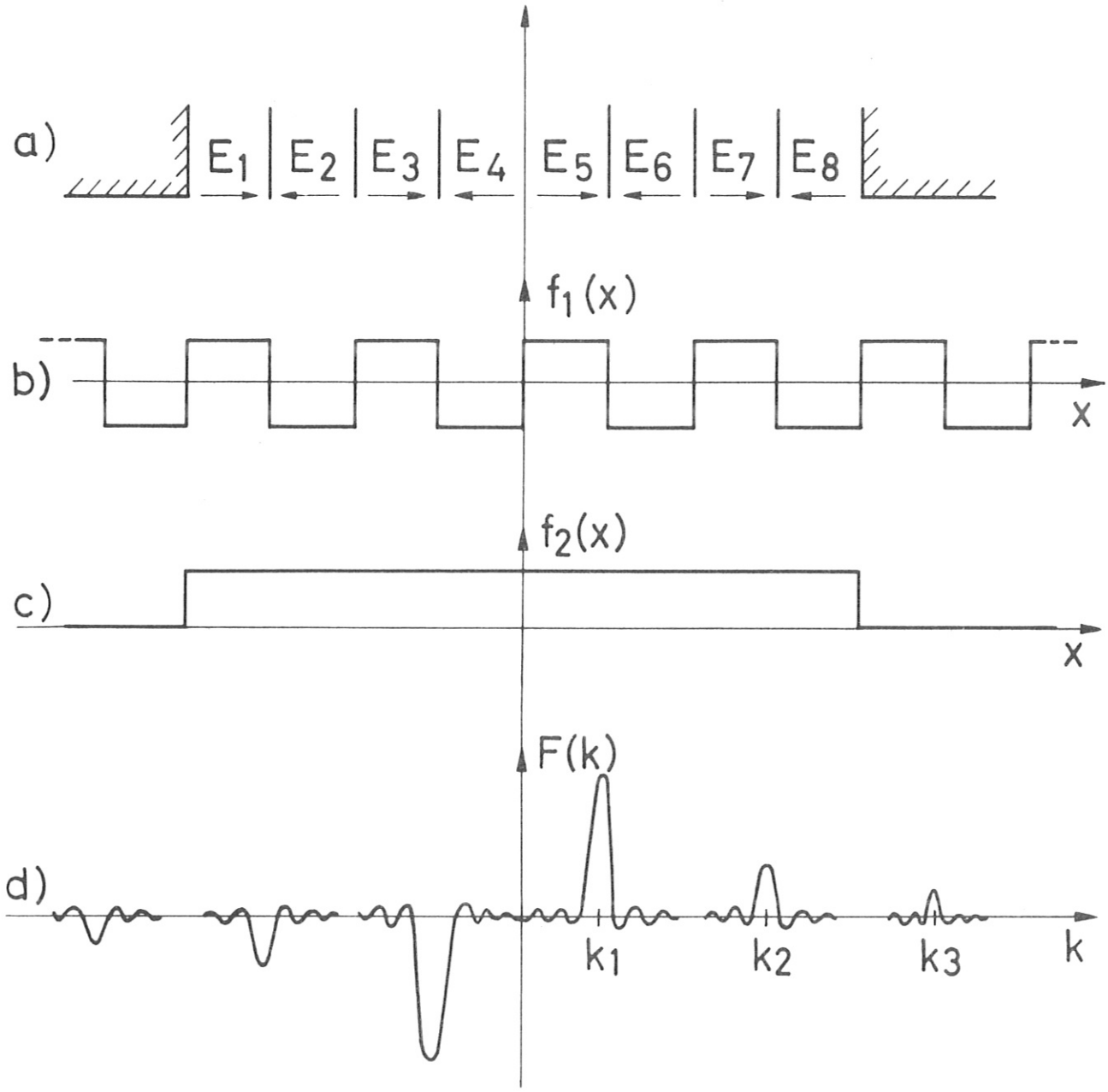

FIG.11

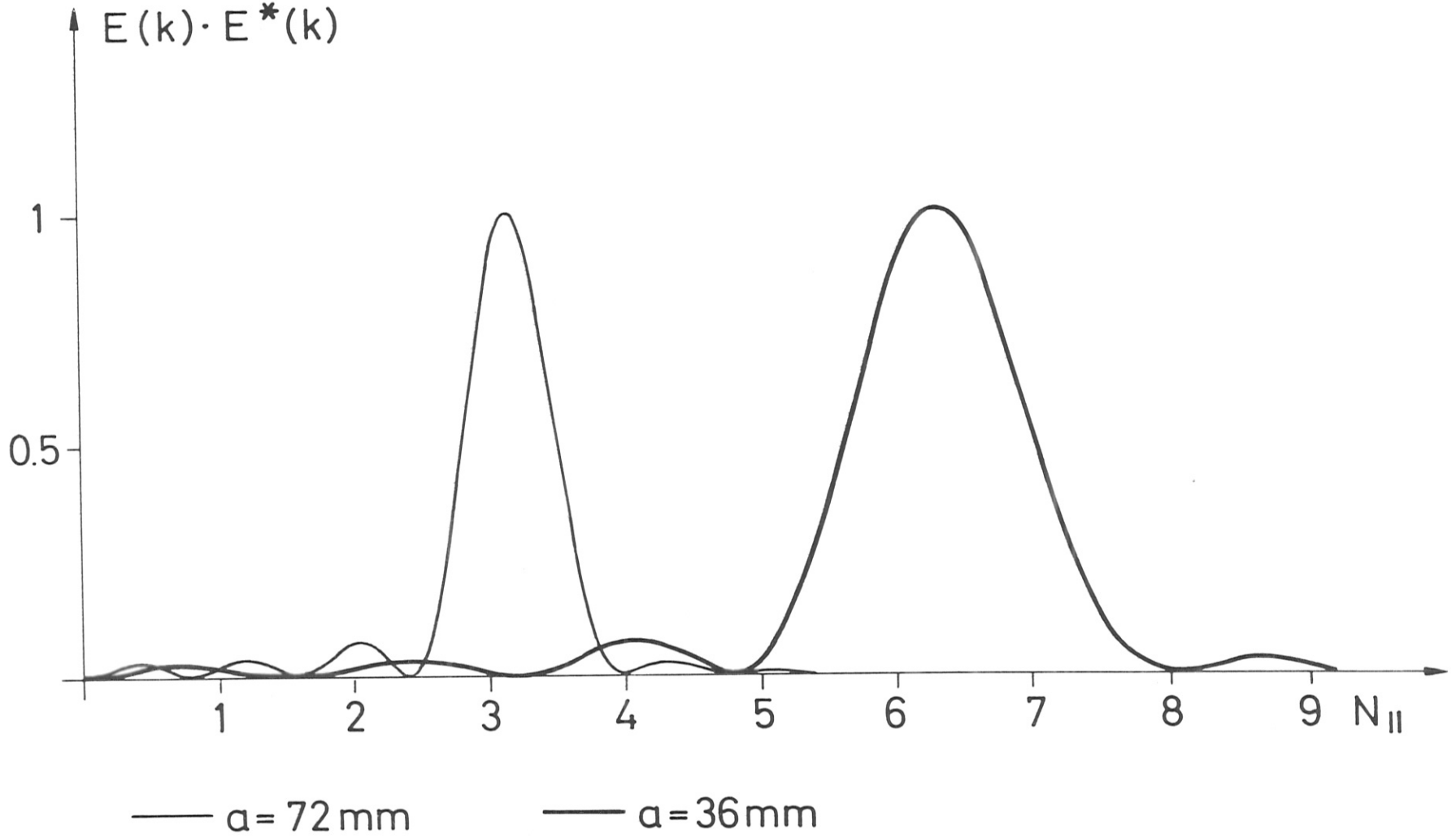

FIG.12

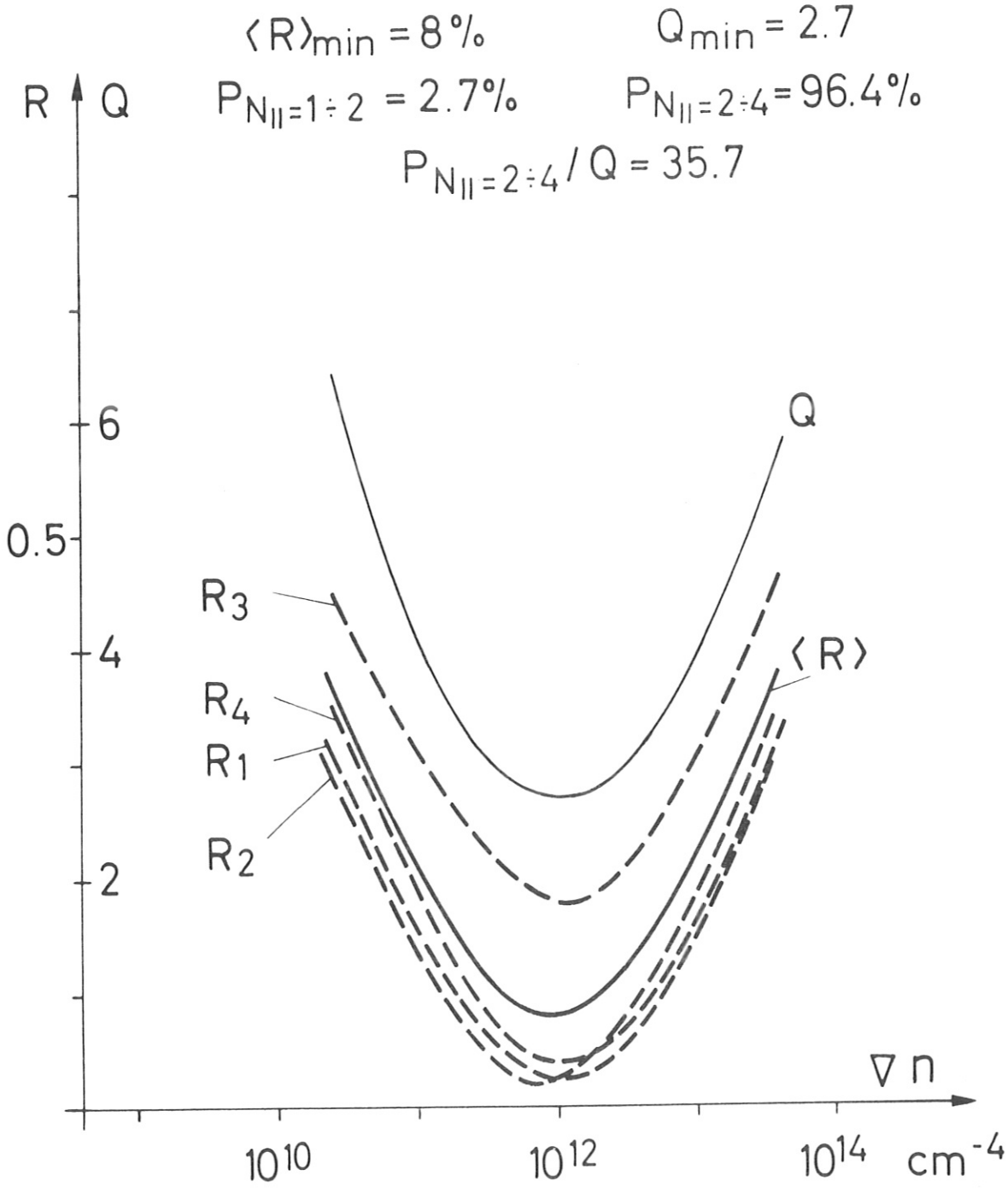
⟨R⟩min = 8%
Qmin = 2.7
R Q
PN||=1÷2 = 2.7%
PN||=2÷4 = 96.4%
PN||=2÷4 / Q = 35.7
6
0.5
4
2
Q
R3
⟨R⟩
R4
R1
R2
∇n
10^10
10^12
10^14
cm^-4

FIG.13A

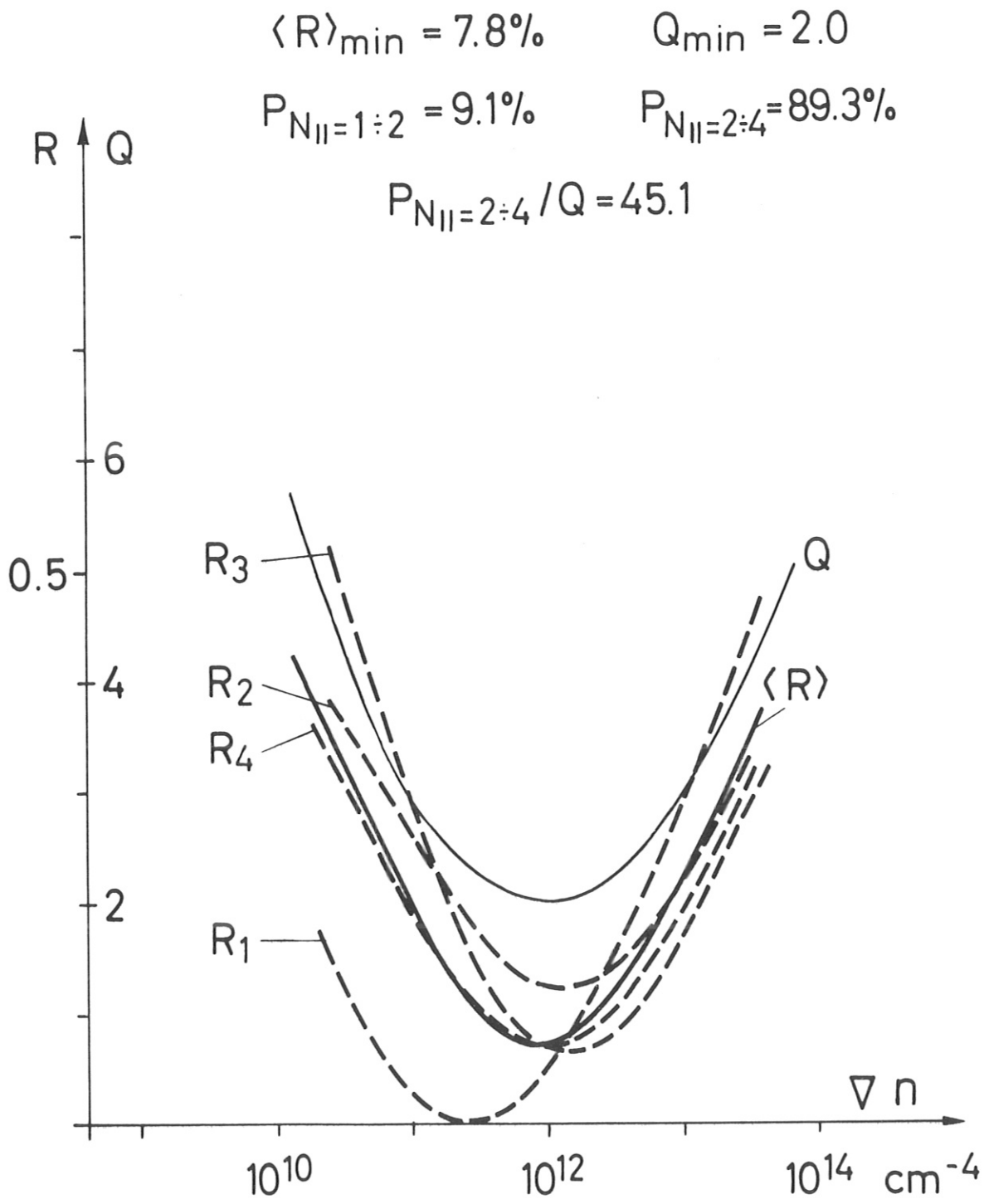
⟨R⟩min = 7.8%
Qmin = 2.0
PNII=1÷2 = 9.1%
PNII=2÷4 = 89.3%
PNII=2÷4 / Q = 45.1
R
Q
6
0.5
4
2
R3
R2
R4
R1
Q
⟨R⟩
∇ n
10^10
10^12
10^14 cm^-4

FIG.13B

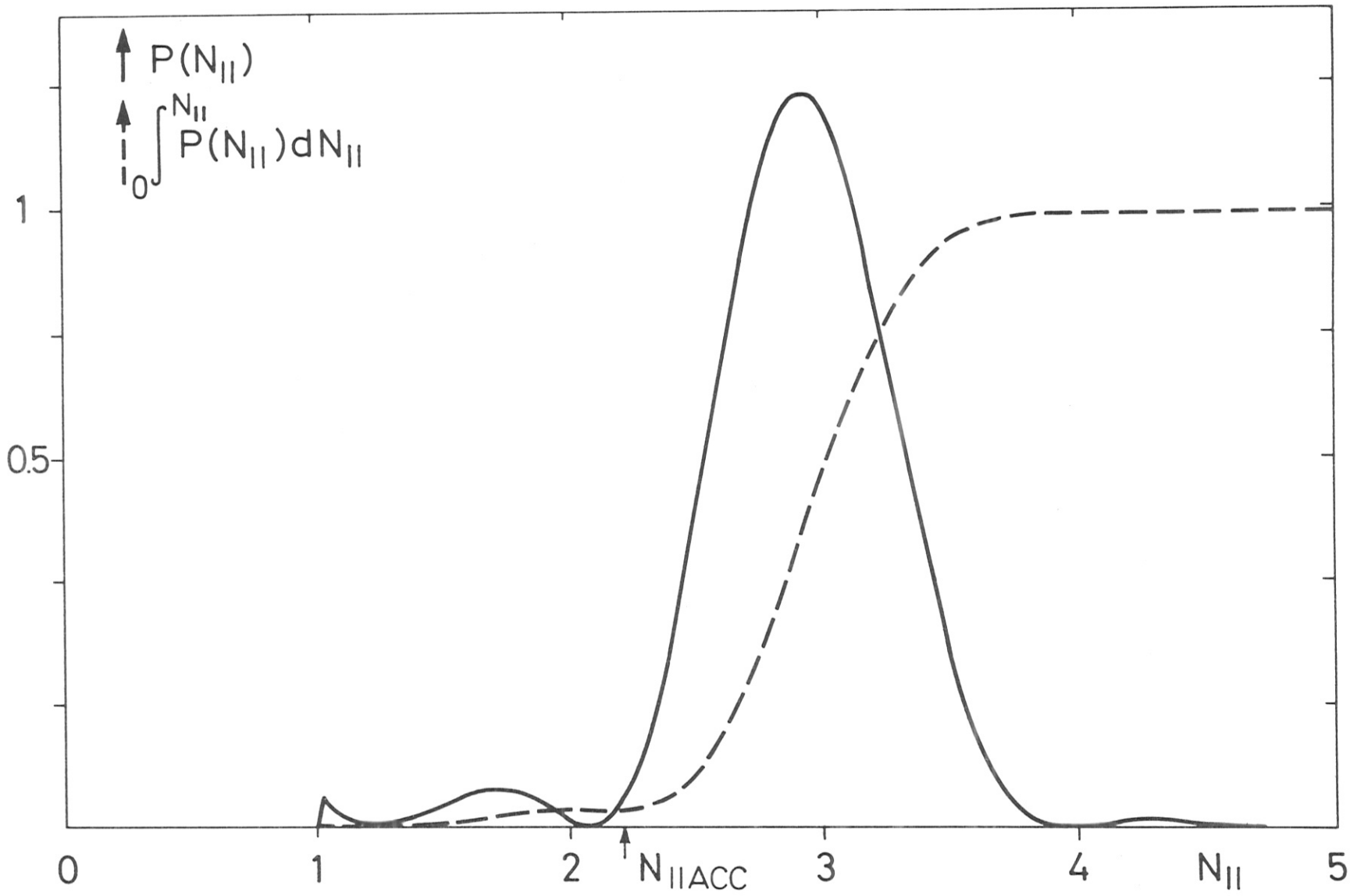

FIG.14

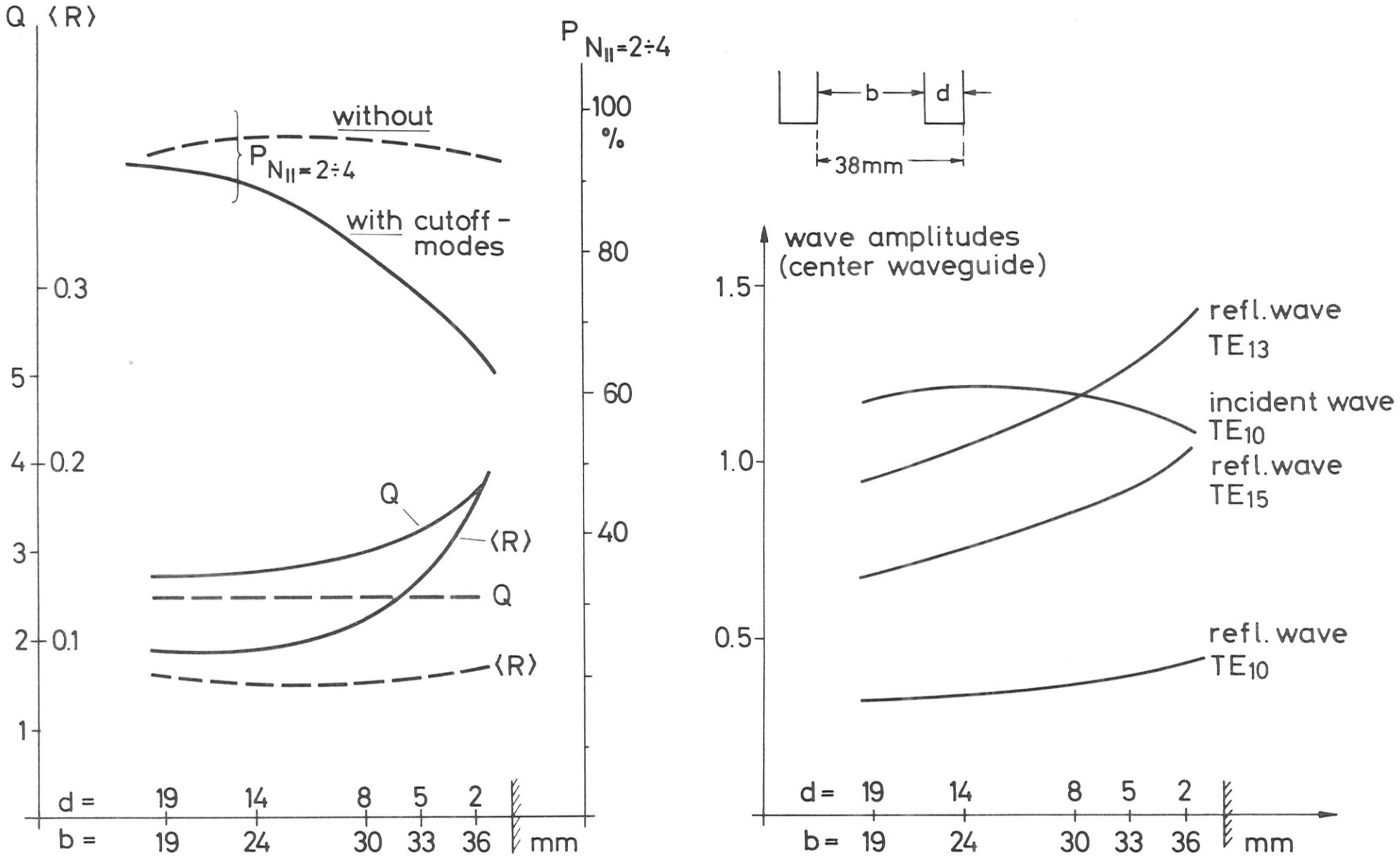
Q ⟨R⟩
P N∥=2÷4
100 %
80
60
40
without
P N∥=2÷4
with cutoff - modes
0.3
0.2
0.1
5
4
3
2
1
Q
⟨R⟩
Q
⟨R⟩
d = 19 14 8 5 2
b = 19 24 30 33 36 mm
b
d
38mm
wave amplitudes
(center waveguide)
1.5
1.0
0.5
refl.wave TE13
incident wave TE10
refl.wave TE15
refl.wave TE10
d = 19 14 8 5 2
b = 19 24 30 33 36 mm

FIG.15